NOAA Technical Memorandum OAR PMEL-141

DEVELOPING TSUNAMI FORECAST INUNDATION MODELS FOR HAWAII: PROCEDURES AND TESTING

Liujuan Tang[1,2]
Christopher D. Chamberlin[1,2]
Vasily V. Titov[1,2]

[1]Joint Institute for the Study of the Atmosphere and Ocean (JISAO)
University of Washington, Seattle, WA

[2]Pacific Marine Environmental Laboratory
Seattle, WA

Pacific Marine Environmental Laboratory
Seattle, WA
August 2008

UNITED STATES DEPARTMENT OF COMMERCE

Carlos M. Gutierrez
Secretary

NATIONAL OCEANIC AND ATMOSPHERIC ADMINISTRATION

VADM Conrad C. Lautenbacher, Jr.
Under Secretary for Oceans and Atmosphere/Administrator

Office of Oceanic and Atmospheric Research

Richard W. Spinrad
Assistant Administrator

NOTICE from NOAA

Mention of a commercial company or product does not constitute an endorsement by NOAA/OAR. Use of information from this publication concerning proprietary products or the tests of such products for publicity or advertising purposes is not authorized. Any opinions, findings, and conclusions or recommendations expressed in this material are those of the authors and do not necessarily reflect the views of the National Oceanic and Atmospheric Administration.

Contribution No. 2985 from NOAA/Pacific Marine Environmental Laboratory

Also available from the National Technical Information Service (NTIS)
(`http://www.ntis.gov`)

Contents

Abstract **1**

1 Background and Objective **1**

2 Forecast Methodology **2**
2.1 Tsunami Source Based on DART Observations and Tsunami Source Functions 4
2.2 Real-Time Site-Specific Forecasting by Stand-by Inundation Models 5

3 Developing Forecast Inundation Models for Hawaii **6**
3.1 Regional, Coastal, and Nearshore Grids 6
3.2 Sensitivity Study of Site-Specific Inundation Models to Model Setup 8
3.2.1 Sensitivity of modeled time series to grid resolutions and computational domains 8
3.2.2 Sensitivity of modeled time series to grid coupling schemes 10
3.2.3 Sensitivity of inundation to topography and friction coefficients 10
3.3 Procedures and Testing 13

4 Developing a Forecast Inundation Model for Kahului, Hawaii **14**
4.1 Study Area and Tsunami Data 14
4.2 Bathymetry and Topography 19
4.3 Model Setup 22
4.4 Results and Discussion 23
4.4.1 Validation and error estimate 23
4.4.2 Assessment of potential impact for Kahului from simulated T_{Mw} 7.5, 8.2, 8.7, and 9.3 tsunamis 34
4.4.3 Robustness and stability 39
4.4.4 Inundation tests 39

5 Summary and Conclusions **42**

6 Acknowledgments **44**

7 References **45**

List of Figures

1 Computational domain of the propagation database for the Pacific. 3
2 Forecast inundation model setups in Hawaii 7
3 Tsunami time series computed from different grid setups 9

4	Tsunami time series at Hilo tide gage computed from one- and two-way coupling schemes	11
5	Maximum water elevations at Hilo computed from two sets of topographic and bathymetric grids for the 1946 Unimak tsunami	12
6	Inundations at Pearl Harbor computed from two sets of topographic data sources for a simulated T_{Mw} 9.3 tsunami	13
7	An aerial photo of Kahului	16
8	A map of Kahului	17
9	Population density, Maui	18
10	Bathymetric and topographic data source overview of Hawaiian Islands and Maui	20
11	Grid setup of the Kahului Reference Inundation Model (RIM)	24
12, 1–3	Observed and modeled time series of (a) wave amplitudes and (b, c, and d) wavelet-derived amplitude spectra at Kahului tide gage for the 14 historical tsunamis in Table 4	25
12, 4–6	continued	26
12, 7–9	continued	27
12, 10–12	continued	28
12, 13–14	continued	29
13	Comparison and error estimation of (a) maximum wave height, (b) arrival of the first wave peak, and (c) peak wave period of observations and model results from the Kahului SIM.	33
14, 1–7	Maximum water elevation and maximum velocity computed by the Kahului RIM and SIM for the 14 historical tsunamis.	36
14, 8–14	continued	37
15	Maximum water elevation at (a) Kahului offshore from the propagation database and (b, c, d, and e) at Kahului tide station computed by the Kahului SIM for simulated T_{Mw} 7.5, 8.2, 8.7, and 9.3 tsunamis	38
16	Tsunami time series at the Kahului tide station computed by the RIM and SIM from a set of simulated T_{Mw} 9.3 earthquakes	40
17	Maximum water elevation in the study area generated by the same set of 18 simulated T_{Mw} 9.3 tsunamis as in Fig. 16.	41
18	Sensitivity of inundation and time series of tsunami amplitudes	43

List of Tables

1 Tsunami source functions in the Pacific, Indian, and Atlantic oceans. 5
2 Data sources used for grid development. 21
3 MOST setup of Kahului RIM and SIM. 23
4 Tsunami sources and maximum wave height recorded at Kahului tide station for 14 historical tsunamis. 31
5 Simulated tsunamis for hazard assessment study for Kahului. . . 35

Developing tsunami forecast inundation models for Hawaii: Procedures and testing

L. Tang[1,2], C. Chamberlin[1,2], and V.V. Titov[1,2]

Abstract. This report describes the procedures and testing for developing tsunami forecast inundation models, named Stand-by Inundation Models (SIMs), for Hawaii, as components of NOAA's tsunami forecast and warning system. The activity included sensitivity studies of nearshore tsunami wave characteristics and inundations for ranges of model grid setups, resolutions, and parameters. The SIM covering Kahului, Maui, is used as an example for demonstration of the development process.

The Kahului SIM was validated with 11 historical tsunami water-level records at Kahului tide station. The accuracy of the maximum wave height computed by the SIM is greater than 80% when the observed maximum wave height is greater than 0.5 m, and 50% when the observation is between 0.3 to 0.5 m. The error of the modeled arrival time of the first peak is within ±3% of the travel time. Wavelet analyses indicate that the peak wave period at the station mainly falls into one of three harbor and local resonant periods, near 16, 24, or 34 min (±2 min). This is relevant to the geographic location of the tsunami source. The SIM outputs are also verified with numerical results from a reference inundation model (RIM) with a higher resolution of 1/3 arc-second (10 m). The optimized SIM can accurately provide a 4-hour forecast of first-wave arrival, amplitudes, and a reasonable inundation limit within minutes of receiving tsunami source information constrained by deep-ocean DART measurements. It is capable of reproducing later tsunami waves reflected or scattered by far-field bathymetry that may arrive hours after the first arrival. The Kahului SIM is tested against different scenarios of simulated T_{Mw} 7.5, 8.2, 8.7, and 9.3 tsunamis based on subduction zone earthquakes in the Pacific. It shows robust results for all test cases.

The tsunami hazard assessment study for Kahului indicates that moment magnitude alone is inadequate to provide warning guidance for coastal communities, since it contains information relevant only to the source. The SIMs, which contain local bathymetric and topographic information, and utilize the dynamic boundary conditions from the propagation database, are particularly designed for site-specific forecasts for coastal communities. Only by combining DART-constrained tsunami magnitude with site-specific SIMs can the forecast completely cover the three distinct stages of earthquake-generated tsunamis—generation, deep-ocean propagation, and coastal transformation, including runup.

1. Background and Objective

The NOAA Center for Tsunami Research (NCTR) at NOAA's Pacific Marine Environmental Laboratory (PMEL) is developing a tsunami forecasting system known as Short-term Inundation Forecasting for Tsunamis (SIFT) for NOAA's Tsunami Warning Centers (Titov *et al.*, 2005). The primary goal of the system is to provide NOAA's Tsunami Warning Centers with operational tools that combine real-time deep-ocean tsunami measurements from the Deep-ocean Assessment and Reporting of Tsunami (DART) buoys (González *et al.*, 2005; Bernard *et al.*, 2006; Bernard and Titov, 2007), with the Method of Splitting Tsunami (MOST) model, a suite of finite difference numerical codes based on nonlinear long wave approximation (Titov

[1]Joint Institute for the Study of the Atmosphere and Ocean, University of Washington, Seattle, WA

[2]NOAA, Pacific Marine Environmental Laboratory, Seattle, WA

and Synolakis, 1998; Titov and González, 1997; Synolakis *et al.*, 2007), to produce efficient forecasts of tsunami arrival time, heights, periods, and inundation. To achieve accurate and detailed forecasts on the likely impact of incoming tsunamis on specific sites within certain time limits and to reduce false alarms, Stand-by Inundation Models (SIMs) are being developed for U.S. coastal communities that are potentially most at risk, and integrated as crucial components of the forecast system.

Presently, a system of 35 DART buoys (32 U.S.-, 1 Chilean-, and 2 Australian-owned) is monitoring tsunami activity in the Pacific Ocean (Fig. 1) (44 DART buoys globally). The pre-computed propagation models currently have 899 scenarios to cover Pacific tsunami sources (1299 globally), and the high-resolution forecast inundation models (SIMs) are now set up for 26 U.S. coastal communities. The fully implemented system will use real-time data from the DART network to provide high-resolution tsunami forecasts for at least 75 communities in the U.S. (by 2013) (Titov, 2008). Since its first testing in the 17 November 2003 Rat Island tsunami, the forecast system has produced experimental real-time forecasts for eight tsunamis in the Pacific and Indian oceans (Titov *et al.*, 2005; Wei *et al.*, 2008; Titov, 2008). The forecast methodology has also been tested with the data from nine additional events that produced the deep ocean data.

The present study standardizes procedures and testing for developing real-time forecast inundation models (SIMs) for Hawaii based on sensitivity studies. A detailed SIM development is presented for Kahului, Hawaii. This study also performs tsunami hazard assessment and identifies worst-case scenarios from major subduction zone earthquakes that may have a devastating impact on the study site. A secondary objective is to investigate Kahului harbor and local responses to tsunami waves by wavelet analysis.

The remainder of this report is organized as follows. Section 2 introduces PMEL's tsunami forecast methodology. Section 3 describes coastal and nearshore segment setups for the Hawaiian region, discusses the problems and difficulties encountered during SIM developments in the past, and standardizes the procedures and testing for developing forecast inundation models for Hawaii. A detailed SIM development for Kahului is provided in section 4, including validation, testing for robustness and stability, and hazard assessment. A summary and conclusions are presented in section 5.

2. Forecast Methodology

PMEL's real-time tsunami forecasting scheme is a two-step process: (1) constructing a tsunami source through inversion of deep ocean DART observations utilizing pre-computed tsunami source functions, and (2) real-time site-specific forecasting for coastal communities by SIMs, where MOST operates differently (Titov *et al.*, 1999; 2005).

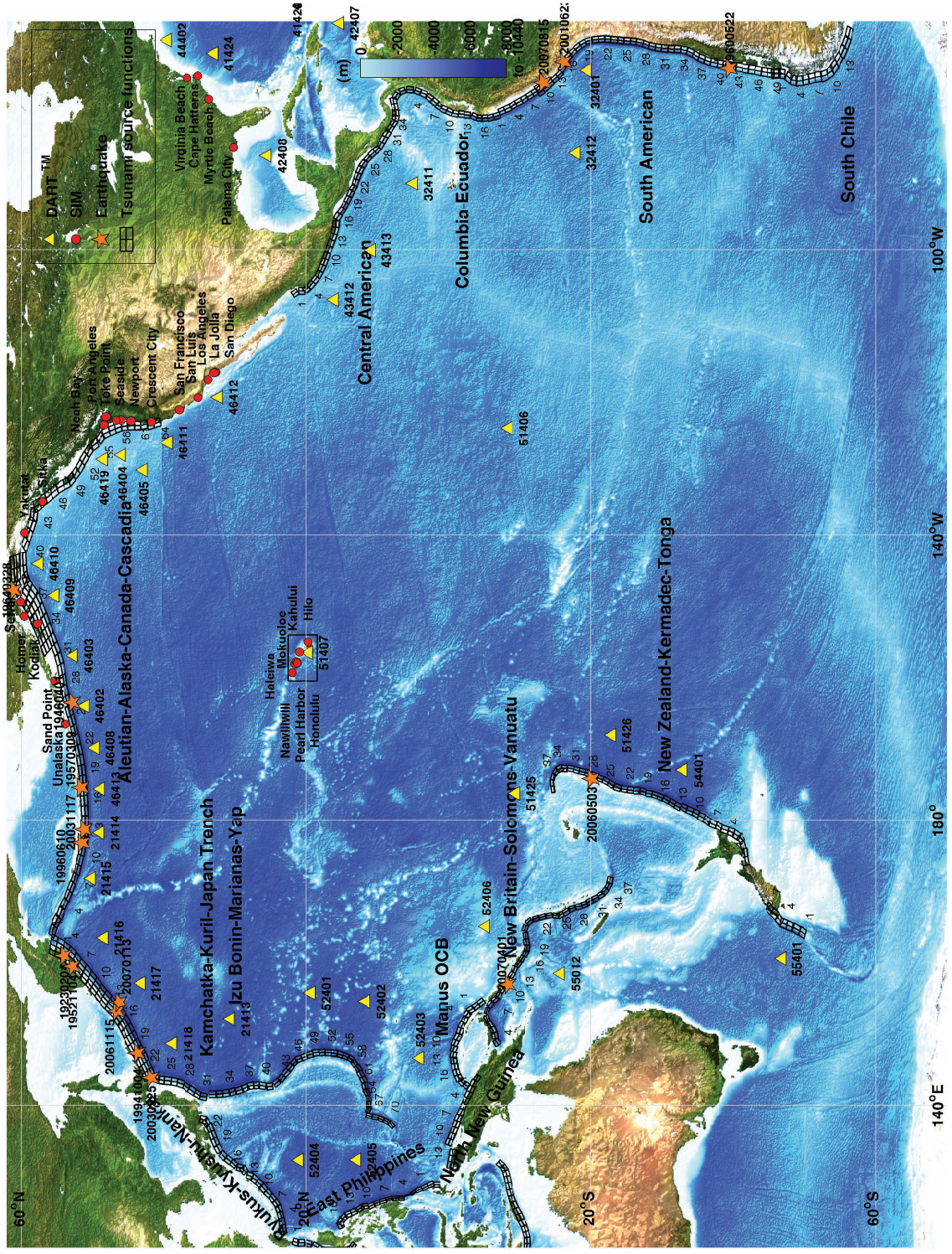

Figure 1: Computational domain of the propagation database for the Pacific.

2.1 Tsunami Source Based on DART Observations and Tsunami Source Functions

A tsunami source refers to an equivalent earthquake that is able to reproduce similar tsunami wave characteristics, including arrival, height, and period, in the deep ocean without knowing details of the earthquake's focal mechanism. The wave dynamics of tsunami propagation in the deep ocean can be approximated using linear theory. Thus a tsunami source can be effectively constructed based on the best fit to given deep-ocean tsunami measurements with pre-computed tsunami source functions.

Titov *et al.* (1999; 2001) conducted sensitivity studies on far-field deep-water tsunamis based on various parameters of commonly used fault plane source models (Gusiakov, 1978; Okada, 1985). The results showed that source magnitude and location essentially define far-field tsunami signals for a wide range of subduction zone earthquakes. Other parameters have a secondary influence and can be ignored during forecast. Based on the results, propagation databases for the Pacific, Atlantic, and Indian oceans have been built using pre-defined source parameters: length = 100 km, width = 50 km, slip = 1 m, rake = 90 and rigidity = 4.5×10^{10} N/m^2. Other parameters are location specific. (Details of the databases are described in Gica *et al.*, 2008.) Each scenario represents a tsunami from a typical M_w = 7.5 earthquake and we refer to it as one tsunami source function (TSF). Figure 1 shows the earthquake locations of tsunami source functions and Table 1 summarizes the databases. Presently, the Pacific database contains 899 TSFs (1299 globally). At each subduction zone, up to five lines of TSFs from seaward to landward, B, A, Z, Y, and X, are placed adjacent to one another. Figure 1 also shows the computational domain of the database in the Pacific, the propagation grid for MOST, which extends from 120°E 70°S to 68°W 62°N, with a resolution of 4 min and a time step of 15 sec. The computational results, including amplitudes and depth-averaged velocities, were saved in the database at every 16 min in space and 60 sec in time.

Several real-time data sources, including seismic, coastal tide gage, and deep-ocean data have been used for tsunami warning and forecast. PMEL's strategy for real-time forecasting is to use deep-ocean measurements at DART buoys as the primary data source based on several key features: (1) They are the direct measure of tsunami waves, unlike seismic data, which are indirect. (2) Compared with coastal tide gages, DART data of high signal-to-noise ratio can be obtained quickly without harbor and instrument responses. (3) The linear process of tsunamis in the deep ocean allows the application of efficient inversion schemes.

Time series of tsunami observations in the deep ocean can be decomposed into a linear combination of a set of tsunami source functions in the time domain by the linear least squares method. We refer to the coefficients obtained through this inversion process as tsunami source coefficients. And the magnitude computed from the sum of the magnitudes of TSFs multiplied by the corresponding coefficients is referred to as the tsunami moment magnitude (T_{Mw}), to distinguish it from the seismic moment magnitude

Table 1: Tsunami source functions in the Pacific, Indian, and Atlantic oceans.

Subduction Zone			Tsunami Source Functions	
No.	**Abbr.**	**Name**	**Line/Zone**	**Numbers**
1	AACC	Aleutian-Alaska-Canada-Cascadia	BAZYX	162
2	CASZ	Central American	BA	72
3	CESZ	Columbia-Ecuador	BA	36
4	EPSZ	East Philippines	BA	38
5	KKJI	Kamchatka-Kuril-Japan Trench-Izu Bonin-Marianas-Yap	BAZY	184
6	MOCB	Manus Ocean Convergence Boundary	BA	34
7	NBSV	New Britain-Solomons-Vanuatu	BA	74
8	NNGZ	North New Guinea	BA	30
9	NZKT	New Zealand-Kermadec-Tonga	BA	78
10	RKNZ	Ryukus-Kyushu-Nankai	BA	44
11	SASZ	South American	BAZY	103
12	SCSZ	South Chile	BA	30
13	NZSZ	South New Zealand	BA	14
			Subtotal:	**899**
14	ATSZ	Atlantic	BA	184
15	ANSJ	Adaman-Nicobar-Sumatra-Java	BAZY	174
16	MKSZ	Makran	BA	20
17	WPSZ	West Philippines	BA	22
			Total:	**1299**

M_w, which is obtained from the moment tensor analysis of seismic waves. The inversion process uses tsunami travel time to locate the source and the observed tsunami amplitudes to constrain the magnitude. Wave period is mainly defined by source location.

The database can provide an offshore forecast of tsunami amplitudes and all other wave parameters around the Pacific immediately once the inversion is complete. The tsunami source, which combines real-time tsunami measurements with TSFs, provides an accurate offshore tsunami scenario without additional time-consuming model runs.

2.2 Real-Time Site-Specific Forecasting by Stand-by Inundation Models

The evolution of earthquake-generated tsunami waves has three distinctive stages: generation, propagation, and coastal transformation, including runup. The SIM is particularly designed for the last stage, which is very important since it provides information on the likely impact of an incoming tsunami on site-specific coastal communities, where lives and properties are at risk. The DART-constrained tsunami source, the corresponding offshore scenario from the propagation database, and the site-specific SIMs cover all three stages, providing a complete tsunami forecast capability.

Tsunami inundation is a highly nonlinear process. Forecasting of the maximum wave height nearshore also requires non-linear inundation models and fine-resolution bathymetry/topographic data. The SIM utilizes the rigorously tested Method of Splitting Tsunami (MOST) model, a finite dif-

ference tsunami inundation model based on nonlinear shallow-water wave equations. Each SIM consists of three telescoping computational grids for regional, coastal, and nearshore areas, with increasing resolution. Runup and inundation are computed within the nearshore grid. The nearshore grid includes the population center and tide stations for forecast verification. The computational grids for SIMs are derived from the best available bathymetry/topographic data at the time of development. Grids will be continuously updated when better bathymetry/topographic data is available.

SIMs are implemented and optimized for speed and accuracy. Once the tsunami source is obtained, the pre-computed time series of offshore wave height and depth-averaged velocity in the propagation database are applied as the dynamic boundary conditions for SIMs, which saves additional computational time for propagation. By reducing the computational areas and grid resolutions, which allows larger time steps without violations of the CFL conditions, SIMs are optimized to provide 4-hour event forecasting results in minutes of computational time using a single processor. To ensure forecast accuracy, SIM outputs are validated and verified with historical tsunami records as well as results from a reference inundation model (RIM) with higher resolutions and extended computational domains. In order to provide warning guidance for a long duration during a tsunami event, each SIM has been tested to output a simulation for up to 24 hours after the tsunami generation.

3. Developing Forecast Inundation Models for Hawaii

3.1 Regional, Coastal, and Nearshore Grids

The forecast setup for Hawaii consists of three layers of telescoping grids as shown in Fig. 2.

(a) One regional grid of 2-arc-min resolution covers the main Hawaiian Islands.

(b) The whole Hawaiian coastline is divided into four coastal grids of 12- to 18-arc-sec for four natural geographic groups:

  (b.1) Niʻihau, Kaʻula Rock, and Kauai (Kauai complex)

  (b.2) Oahu,

  (b.3) Molokai, Maui, Lanai, and Kahoʻolawe (the Maui Complex), and

  (b.4) Hawaii.

(c) Within each coastal grid, the coastline is further divided into 2-arc-sec nearshore grids. Runup and inundation are computed within the nearshore grids, where it has a high concentration of population or activities.

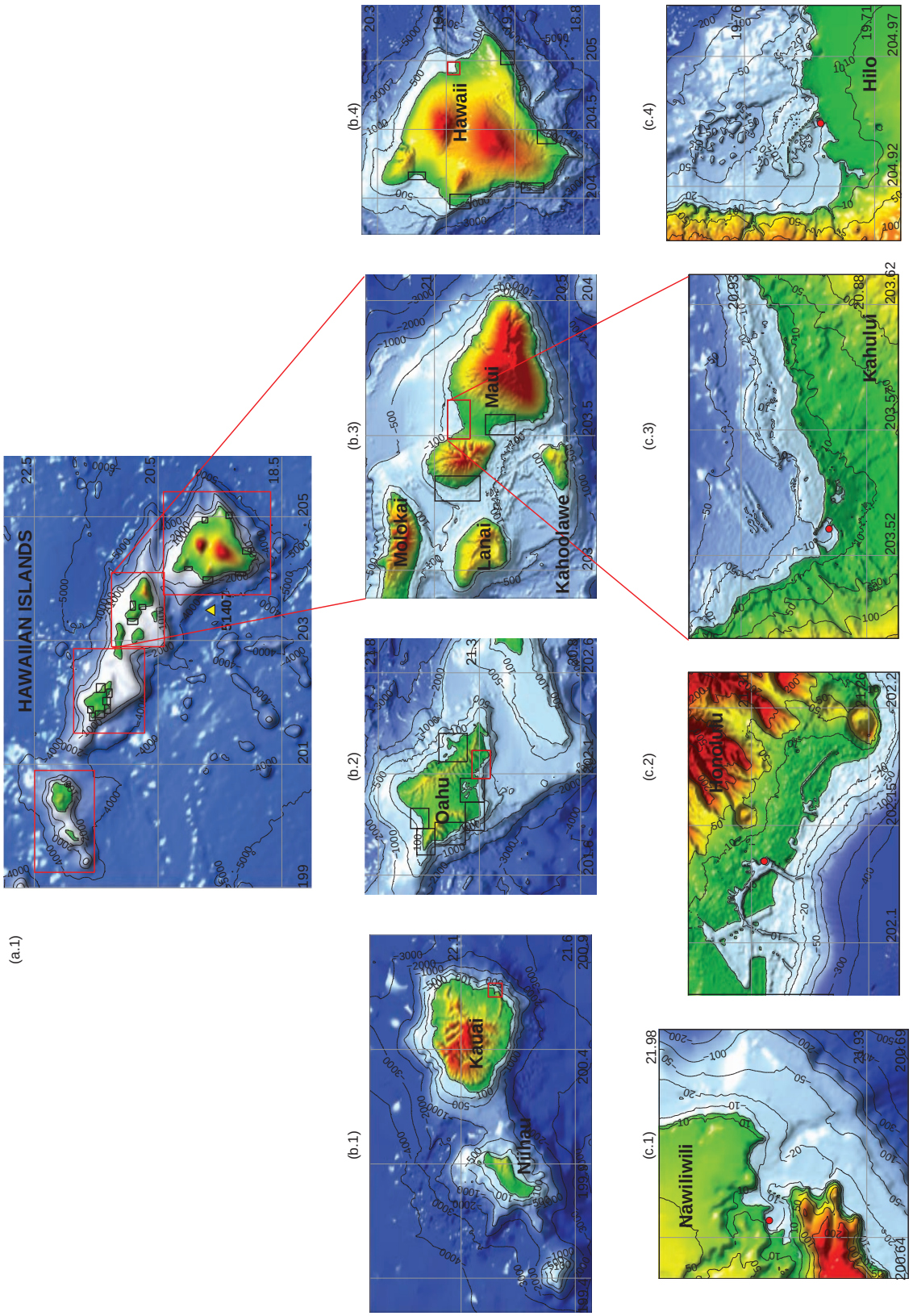

Figure 2: Forecast inundation model setups in Hawaii: (a) regional, (b) coastal, and (c) nearshore grids.

At present, each SIM is independently set up to use three telescoping rectangular grids. NCTR has ongoing research on implementation of the MOST model with curvilinear and multi-nesting grids. SIMs can be set up to utilize the shared regional or coastal grids to improve forecast speed in the future.

3.2 Sensitivity Study of Site-Specific Inundation Models to Model Setup

How sensitive are the model outputs, including time series and inundation, to changes in the grid resolutions, computational domains, accuracy of bathymetry/topography, and other parameters? This issue is central to SIM development, since giving a correct tsunami source and a well-validated tsunami inundation numerical model, with an inappropriate model setup or inaccurate bathymetry/topography, can produce poor results.

3.2.1 Sensitivity of modeled time series to grid resolutions and computational domains

Figure 3 compares results from different model setups for Kahului, Honolulu, and Los Angeles. Setup 3 has resolutions of $120''$, $24''$, and $3''$ for the Kahului regional, coastal, and nearshore grids (Fig. 3a). The observed maximum wave amplitude is 25 cm during the 2006 Tonga tsunami, while the modeled maximum amplitude in setup 3 is only 11 cm (-56% error). With a higher resolution of $12''$ and an extended computational domain applied to the coastal grid, which includes portions of nearby Molokai, Lanai, and Kahoʻolawe islands, setup 2 produces a 21-cm maximum amplitude. For a 4-hour simulation, the computational time increases from about 8 min for setup 3 to 10 min for setup 2. Further increasing grid resolutions to $36''$, $6''$, and $1''$ as in setup 1 produces a 28-cm maximum amplitude. Meanwhile the computational time increases to about 8 hours. Prior to the 2006 Tonga tsunami, setup 3 was tested with six historical events, the 2003 Rat Island, 2003 Hokkaido, 1996 Andreanof, 1994 East Kuril Island, 1964 Alaska, and 1957 Andeanof tsunamis. It produced good comparisons to the observations at the Kahului tide station. However, when the 2006 Tonga tsunami came from a direction from which neither data exists nor a test had been done before, the hidden deficiency of setup 3 was exposed. Therefore, to ensure the computational domains for SIMs, including the appropriate bathymetry features, and as a consequence, to provide the right boundary conditions for modeling of wave scattering, it is important to test Hawaiian SIMs with tsunamis from all potential directionalities.

In Fig. 3b, grid setup 2 of finer resolution for Honolulu shows a better comparison of wave height and phase for later waves than those of setup 3 for the 1964 Alaska tsunami. While it takes less than 10 min for a 4-hour simulation for setups 2 and 3, it takes about 64 hours for the finest grid setup 1. The finer the resolution, the better the detail of the fine structures of Honolulu harbor.

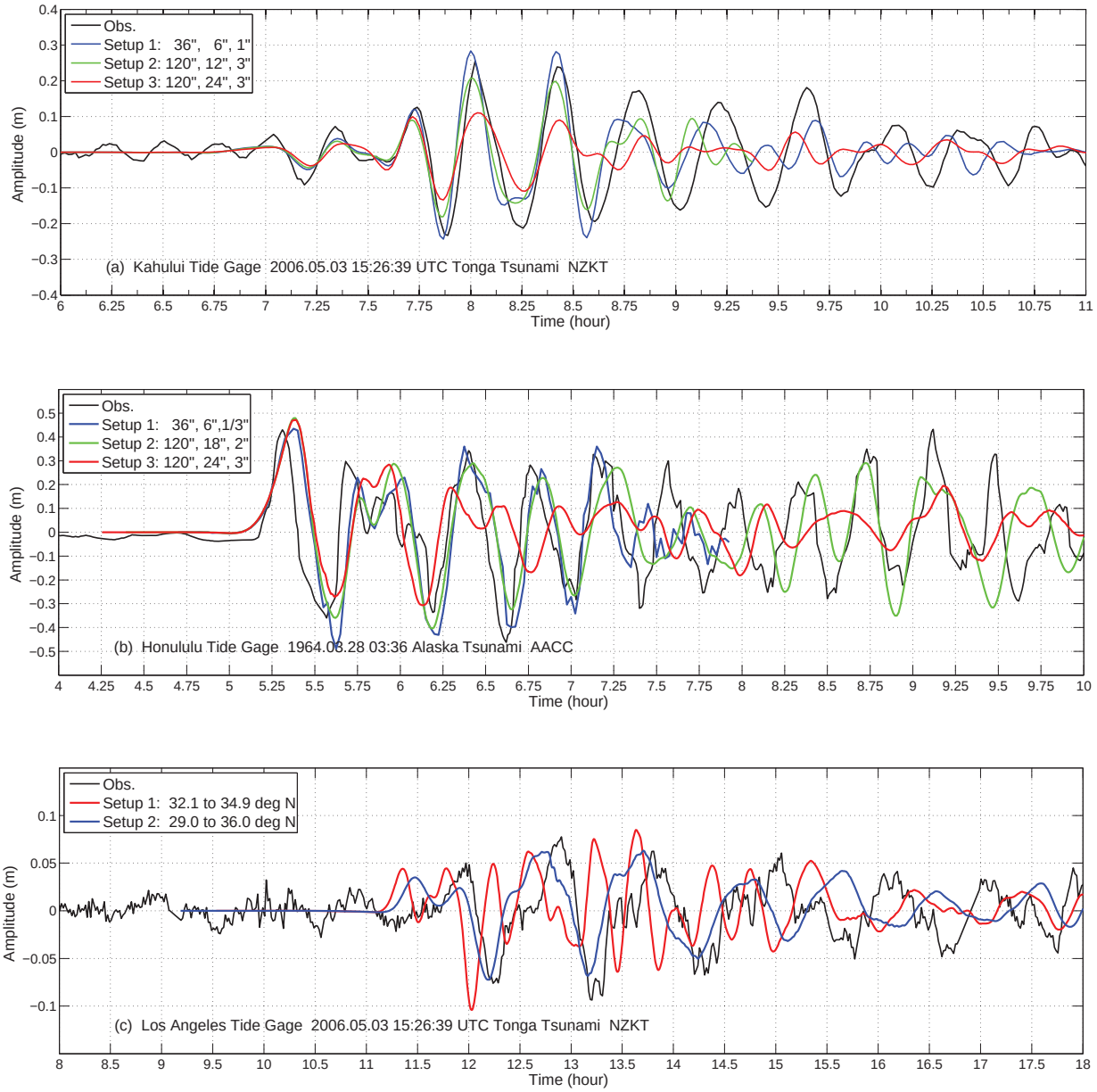

Figure 3: Tsunami time series computed from different grid setups at (a) Kahului tide gage for the 2006 Tonga tsunami, (b) Honolulu tide gage for the 1964 Alaska tsunami, and (c) Los Angeles tide gage for the 2006 Tonga tsunami.

Figure 3c presents an 8-min difference in the arrival time of the first peak from two model time series at Los Angeles tide station for the 2006 Tonga tsunami. The 2-arc-min offshore grid for setup 2 was further extended to the south of Los Angeles to include some shallow bathymetric features. It produces better agreement with the observations when the tsunami propagates from the southwest.

Forecast inundation models need to balance between speed and accuracy. One important guideline in developing tsunami forecast models is to remain within acceptable time limits, using the highest resolution and largest computational domains possible.

3.2.2 Sensitivity of modeled time series to grid coupling schemes

MOST version 1.0 employs a two-way coupling scheme. The coupling is achieved at each time step in the same way that coarse-to-fine resolution level boundary conditions are interpolated from the low-resolution field, and vice versa. The two-way coupling scheme has relatively rigorous requirements for bathymetric consistency as well as time steps between adjacent grids. One example is that water depth at the same location offshore of north Oahu differs by 400 m at 2000-m water depth from two different bathymetric data sources. These two sources were applied to construct the regional and coastal grids, respectively, for Honolulu. With the northern boundary in the coastal grid lying through such sudden changes of water depth, boundary instabilities were developed right from the beginning of the model run. Furthermore, even with a consistent bathymetric data source, time steps for the three telescoping grids still need to be carefully tested in order to provide stable model runs of long duration. To overcome these difficulties, a one-way coupling scheme was employed in MOST version 2.0, e.g., there was no interpolation of the fine-resolution field to the coarser resolution level, for forecast purposes. The one-way coupling scheme is robust and can handle bathymetric grids from varieties of data sources with any time steps that satisfy CFL conditions. MOST version 2.0 passed the bench mark tests and in general provided good comparisons with model results from version 1.0. However, there is one exception: so far, we have seen that one-way coupling overestimates the amplitude of the 3rd trough and the 4th peak at Hilo tide station for two events, the 2006 Kuril Islands and 2003 Rat Island tsunamis (Fig. 4). The reason is still under investigation. We suggest double checking forecast results for the Hilo SIM by using the two-way coupling scheme.

3.2.3 Sensitivity of inundation to topography and friction coefficients

Accurate simulation of tsunami run-up and inundation requires high quality run-up and inundation data, high-resolution bathymetry and topography data in the runup area, and good tsunami source parameters. Titov *et al.* (2005) have shown that, under these conditions, the MOST runup and inundation agree quite well with the stereo aerial photo data and filed survey data on Okushiri Island from the 12 July 1993 Hokkaido-Nansei-Oki $M_w = 7.8$ earthquake.

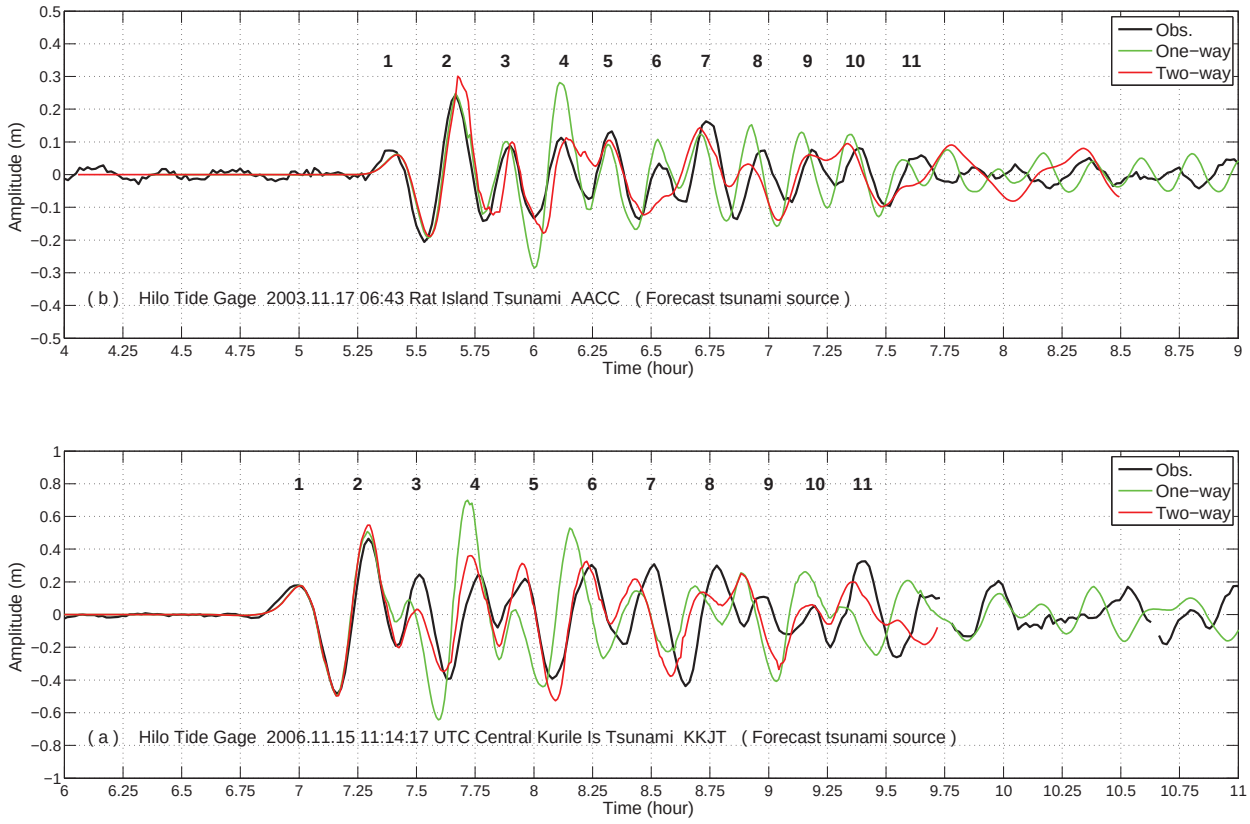

Figure 4: Tsunami time series at Hilo tide gage computed from one- and two-way coupling schemes for (a) the 2006 Kuril Islands tsunami and (b) the 2003 Rat Island tsunami.

At present, one major difficulty in inundation forecasting is lack of high-quality inundation/runup measurements to verify the topographic accuracy and to calibrate the friction coefficient.

Topography/bathymetry compiled with incorrectly aligned datum or from different data sources can produce different inundation results. Figures 5a and 5b show the inundation computed from two sets of grids with the same nearshore 2-arc-sec resolution at Hilo for the 1946 Unimak tsunami. Grid 2 correctly reproduced the inundation limit as shown in Fig. 5c, while no inundation was produced in Grid 1 (Fig. 5a). The topographic 0-, 2-, 5-, and 10-m contours are quite different between these two grids. Developed in 2006 for the Hilo SIM, all data sources for Grid 2 were converted to WGS 84 horizontal geodetic datum and mean high water vertical datum, when necessary. Whether or not the data sources in Grid 1 were converted to the same datum was unclear.

Figures 6a and 6b show that two topographic data sources produced different inundation results along the coastline from Ewa Beach to the Pearl Harbor entrance from a simulated T_{Mw} 9.3 tsunami on the Solomon subduction zone near Santa Cruz Islands. Both nearshore grids have 1/3-arc-sec (10-m) resolution. The high-resolution recent topographic LIDAR from NOAA Coastal Service Center was applied in Grid 2, which was derived for

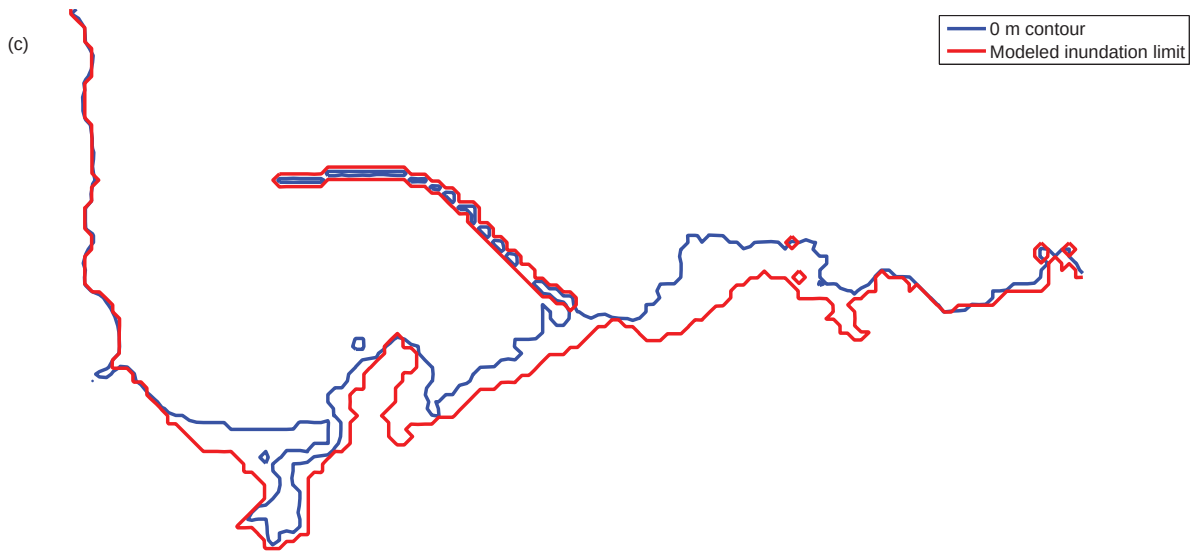

Figure 5: (a) and (b) Maximum water elevations at Hilo computed from two sets of topographic and bathymetric grids for the 1946 Unimak tsunami. (c) Comparison between computed inundation in (b) and measurements from Shepard *et al.* (1950).

Figure 6: Inundations at Pearl Harbor computed from two sets of topographic data sources for a simulated T_{Mw} 9.3 tsunami. Topography in (a) was derived from USGS DEM and (b) from CSC LIDAR data. Color represents the maximum water elevation in meters.

the tsunami hazard assessment study for Pearl Harbor (Tang *et al.*, 2006). The LIDAR data has a "tested 16.9 cm fundamental vertical accuracy at 95 percent confidence level in open terrain," with nominal Ground spacing of 2 m (`http://maps.csc.noaa.gov`). The data was processed to bald earth and interpolated to a 10-m gridded data. The topographic data for Grid 1 was derived from the USGS 7.5-min DEM based on 30-m data spacing. The major 2-, 5-, and 10-m contours agree reasonably well for these two data sets. However, the shore LIDAR data show a long narrow dune with an elevation around 2 m along Ewa Beach, which is absent in the USGS DEM. This results in the difference in inundation seen in Fig. 6. A coastline with long narrow dunes is a common feature in the Hawaiian Islands. Attention must be paid to such features during SIM development. Details of the data sources for Grid 2 can be found in Tang *et al.* (2006).

As will be discussed in Section 4.4.4, a small Manning coefficient such as $n = 0.01$ can produce further inundation at certain flat areas for some test cases.

3.3 Procedures and Testing

The sensitivity study in the previous section provides lessons and guidance for developing site-specific tsunami forecast inundation models. The studies demonstrate that for a fixed tsunami source and a well-validated numerical tsunami inundation model:

(1) Model setups, including grid resolutions and computational domains, are the key factors in accurately modeling the maximum wave height and arrival time nearshore. Other factors, such as tsunami directionalities and grid coupling schemes, may have effects on certain sites for certain events.

(2) Inundation is strongly dependent on the accuracy and spatial resolution of the topography. A small friction coefficient may produce further inundation at some flat areas for some test cases.

Based on the above results, procedures and testing for SIM development are suggested as followed:

(1) *Bathymetry and topography.* Derive DEMs from the best available bathymetric and topographic data sources at the time of development. Update DEMs when a better source is available.

(2) *Resolutions and computational domains.* Within acceptable computational time limits, apply the highest resolutions and largest computational domains for the SIM. Develop a Reference Inundation Model (RIM) of higher resolutions and extended computational domains for each SIM to provide numerical references for the SIM. Include bathymetric and topographic features within or close to the forecast site in the computational domains, such as nearby islands or long narrow dunes along coastlines, to provide correct coastal boundary conditions.

(3) *Validation and verifications.* Validate and verify both the SIM and RIM with all available historical tsunami data, including tide gage records and inundation/runup measurements. Coastal tide gage data are available for Hawaii from fourteen tsunamis since 1946 (Table 4). Test the sensitivity of inundation to a range of friction coefficients.

(4) *Robustness and stability.* Test the SIM and RIM with different scenarios of simulated tsunamis based on major subduction zone earthquakes from all possible directionalities relative to the main Hawaiian Islands. Verify the SIM results with those of the RIM to ensure robustness. Test the SIM for stability up to 24-hour model runs for both historical and simulated scenarios of great subduction zone tsunamis.

A detailed SIM development for Kahului following the above procedures is described in the next section.

4. Developing a Forecast Inundation Model for Kahului, Hawaii

4.1 Study Area and Tsunami Data

The main Hawaiian Islands are the younger and southern portion of the Hawaii Archipelago. From northwest to southeast, the islands form four natural geographic groups by shared channels and an inter-island shelf, including (1) Niʻihau, Kaʻula Rock, and Kauai (Kauai complex) (2) Oahu, (3) Molokai, Maui, Lanai, and Kahoʻolawe (the Maui Complex), and (4) Hawaii. Kahului is located at the north shore of Central Maui and is the largest town on Maui. It hosts Maui's main airport, Kahului Airport, deep-draft harbor, Kahului Harbor, light industrial areas, and commercial shopping centers. Figure 7 presents an aerial photo of this area and a map is shown in Fig. 8. The population density data in Fig. 9 indicates a high concentration of population in Kahului.

The coastal geological features around the Island of Maui are complex. Maui is surrounded to the northwest, west, and south by three smaller islands nearby, Molokai, Lanai, and Kahoolawe, with three channels in between (Fig. 11b). These three channels, Pailolo Channel, Auau Channel, and Alalakeiki Channel have narrow widths of 12.9 km (8 miles), 15 km (9.2 miles), and 11 km (7 miles), respectively. Most portions of the channels are quite shallow, with water depth of less than 300 m. Certain sections of the Auau Channel, which connects Maui and Lanai, are less than 50 m deep. To the southeast, the 48-km-wide (26-mile), 2-km-deep Alenuihaha Channel separates Maui from the Big Island of Hawaii. The island of Maui is unprotected against waves from north and northeast.

The Kahului nearshore is gently embayed, with an average slope of 0.016 from the 0-m down to the 500-m depth contour. On the land, a narrow flat isthmus unites Maui's dominant geological features, two volcanoes, Haleakala (on eastern Maui) and the West Maui Mountains. The isthmus is 11 km (7 miles) across, with the highest elevation of less than 40 m. Other portions of the northern coast of Maui consists generally of cliffs. Coral reefs in shallow water of 1 to 3 feet are as much as 1.2 miles (1.8 km) wide in the study area. The study area covers the coastal communities of Kahului, Wailuku, and Waiehu along the north shore of central Maui, Hawaii. The location of the Kahului tide station is chosen as the warning point (Fig. 8).

Established 19 December 1946 in Kahului Harbor, Kahului tide station has provided valuable records of historical tsunamis. A gas-purging pressure tide gage, also known as the bubbler gage, was installed in 1946. The data was initially recorded on a pen and ink strip chart (Little, 2006). In the mid-1970s this equipment was replaced with an ADR (Analog to Digital Recorder) that used a digital paper punch and recorded the height of water level at 6-min intervals. In February 1989, the Kahului gage was replaced with the Next Generation Water Level Measurement System (NGWLMS). The new primary water-level sensor is an air acoustic measurement device. It is both self-calibrating for variations in the speed of sound, and can be leveled directly to a local benchmark that provides absolute measurements referenced to the local water-level datum. It employs a less restrictive protective well with parallel plates, which only screens out waves with a period shorter than 2–3 sec. The new system's data sampling procedures in conjunction with the open protective well is a significant improvement over the old one (NOAA/NOS, 1991). In 2005, the Kahului tide station was upgraded to one of the tsunami-capable tide stations by NOS/CO-OPS, with new hardware and software to enable the collection and dissemination of 1-min water-level sample data (`http://tidesandcurrents.noaa.gov/1mindata.shtml`). The stations also sample 15-sec data, which can be downloaded later. The MHW at the Kahului tide station is 1.313 m and the MSL is 1.075 m (`http://tidesandcurrents.noaa.gov/`). The mean range of tide is 0.478 m.

Kahului has a long history of destructive tsunamis. The earliest record of a destructive tsunami at Kahului was on 7 November 1837, when the sea first receded horizontally 36 m and then a wall of returning water generated by a wave from southern Chile engulfed inhabitants who were collecting

Figure 7: An aerial photo of Kahului (`http://www.soest.hawaii.edu/coasts/`).

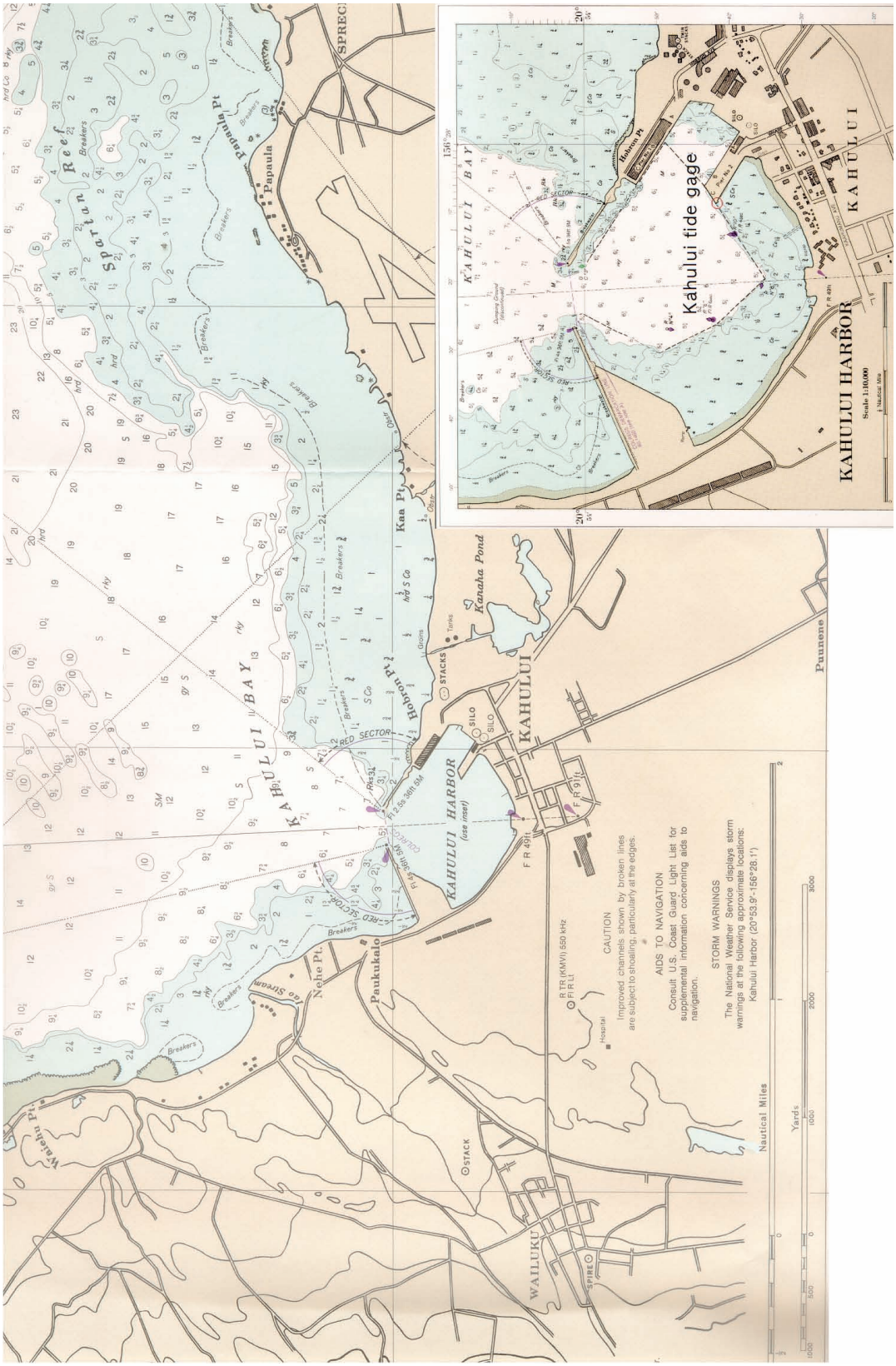

Figure 8: A map of Kahului. Inset: Red circle, Kahului tide gage (the warning point).

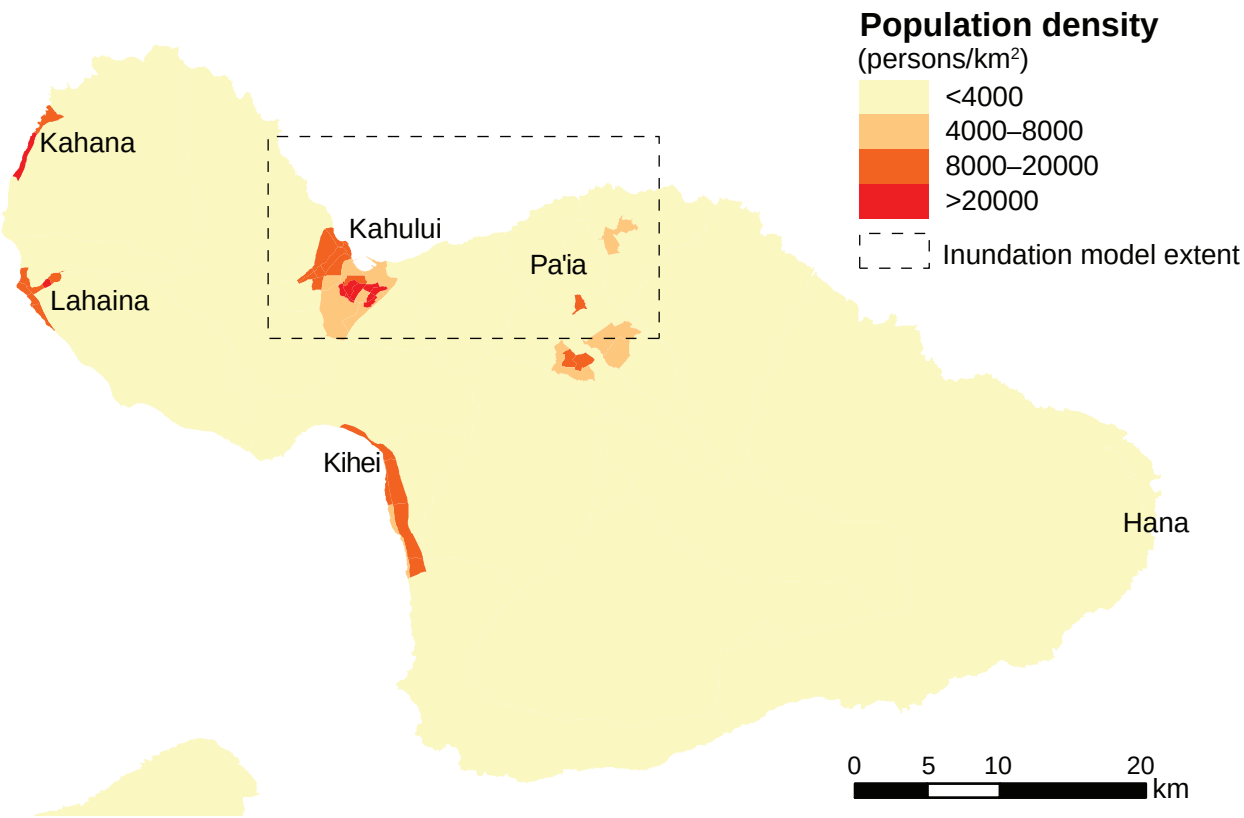

Figure 9: Population density, Maui (Source: 2000 Census).

stranded fish (Pararas-Carayannis, 1969). Two people were drowned and the rest swam to safety. Twenty-six grass houses were carried about 240 m inland. Since 1813, 54 tsunamis have been observed in Kahului, including 23 tsunamis during the period of 1813 to 1968 (a total of 85 tsunamis were observed in the Hawaiian Islands during this period, but unfortunately many of them have no record for Kahului) (Pararas-Carayannis, 1969), 11 between 1969–1982 (Soloviev *et al.*, 1992), 3 during 1983 to 1991, and at least 17 from 1992 to the present. Many of them caused significant damage.

The 3 February 1923 East Kamchatka tsunami caused "heavy damage in Kahului and east coast of Maui." The 1 April 1946 Unimak Island tsunami has the highest tsunami run-up records in the study area among the tsunamis in Table 4. Coral blocks as large as 4 feet in diameter were thrown on shore just east of the breakwater (Shepard *et al.*, 1950). At Spreckelsville the wave reached an elevation of 28 feet and swept inland as far as 800 feet. After that, Kahului tide gage was installed at the northwest corner of pier 2 in Kahului Harbor. "The Kahului-Spreckelsville region suffered the greatest damage" from the 4 November 1952 tsunami from East Kamchatka. On 9 March 1957, the Andreanof tsunami event exceeded the Kahului gage limit of 1.7 m, resulting in considerable damage along the northeast of the Island of Maui (Salsman, 1959). The maximum wave height of the 22 May 1960 South Chile tsunami exceeded the Kahului gage limit of 2.8 m. On 28 March

1964, the gage recorded a maximum wave height of 3.35 m (peak to trough) during the Alaska tsunami. The shopping center near the waterfront was flooded and the total damage was $52,590 in Kahului (Pararas-Carayannis, 1969).

As a population center that has been repeatedly affected by Pacific tsunamis, Kahului is in need of a stand-by inundation model for tsunami forecasting to aid site-specific evacuation decisions.

4.2 Bathymetry and Topography

Tsunami inundation modeling requires accurate bathymetry in coastal areas as well as high-resolution topography and bathymetry in nearshore areas. Two gridded digital elevation models (DEMs) were developed, a bathymetric DEM at medium resolution (6 arc-sec) for wave transformation from the open ocean to coastal areas; and a high resolution (1/3 arc-sec) topography and bathymetry DEM for modeling wave runup and inundation onto dry land. The grids were compiled from several data sources; Fig. 10 is an overview of the spatial extents of each data source used. In areas where multiple datasets overlapped, higher-resolution and newer datasets were generally preferred, and superseded datasets were used for comparison and verification. Table 2 is an overview of the data sources used; in general, the data sources listed first superseded data sources listed later when they overlapped.

Source details for the datasets incorporated into the model grids:

- Joint Airborne Lidar Bathymetry Technical Center of Expertise (JALBTCX), U.S. Army Corps of Engineers, Mobile District. Online reference: `http://shoals.sam.usace.army.mil/hawaii/pages/Hawaii_Data.htm`.
- Monterey Bay Aquarium Research Institute (MBARI) Hawaii Multibeam Survey, Version 1. Online reference: `http://www.mbari.org/data/mapping/hawaii/`.
- USGS Pacific Seafloor Mapping Project. Online reference: `http://walrus.wr.usgs.gov/pacmaps/data.html`.
- Japan Agency for Marine-Earth Science and Technology (JAMSTEC) 1998–1999 multibeam bathymetric surveys. Published in: Takahashi, E. *et al.* (eds.) (2002): Hawaiian Volcanoes: Deep Underwater Perspectives. American Geophysical Union Monograph 128.
  JAMSTEC trackline data was recorded by the R/V *Mirai* during transits in 1999 and 2002. Online reference: `http://www.jamstec.go.jp/mirai/index_eng.html`.
- United States Army Corps of Engineers (USACE), Honolulu District. Online reference: `http://www.poh.usace.army.mil/`.
- NOAA National Geophysical Data Center (NGDC). Online reference: `http://www.ngdc.noaa.gov/mgg/gdas/gd_sys.html`.
- NOAA National Ocean Service (NOS). Sounding points were digitized from NOS nautical charts 19347, 19358, 19359, 19364, 19366, 19342,

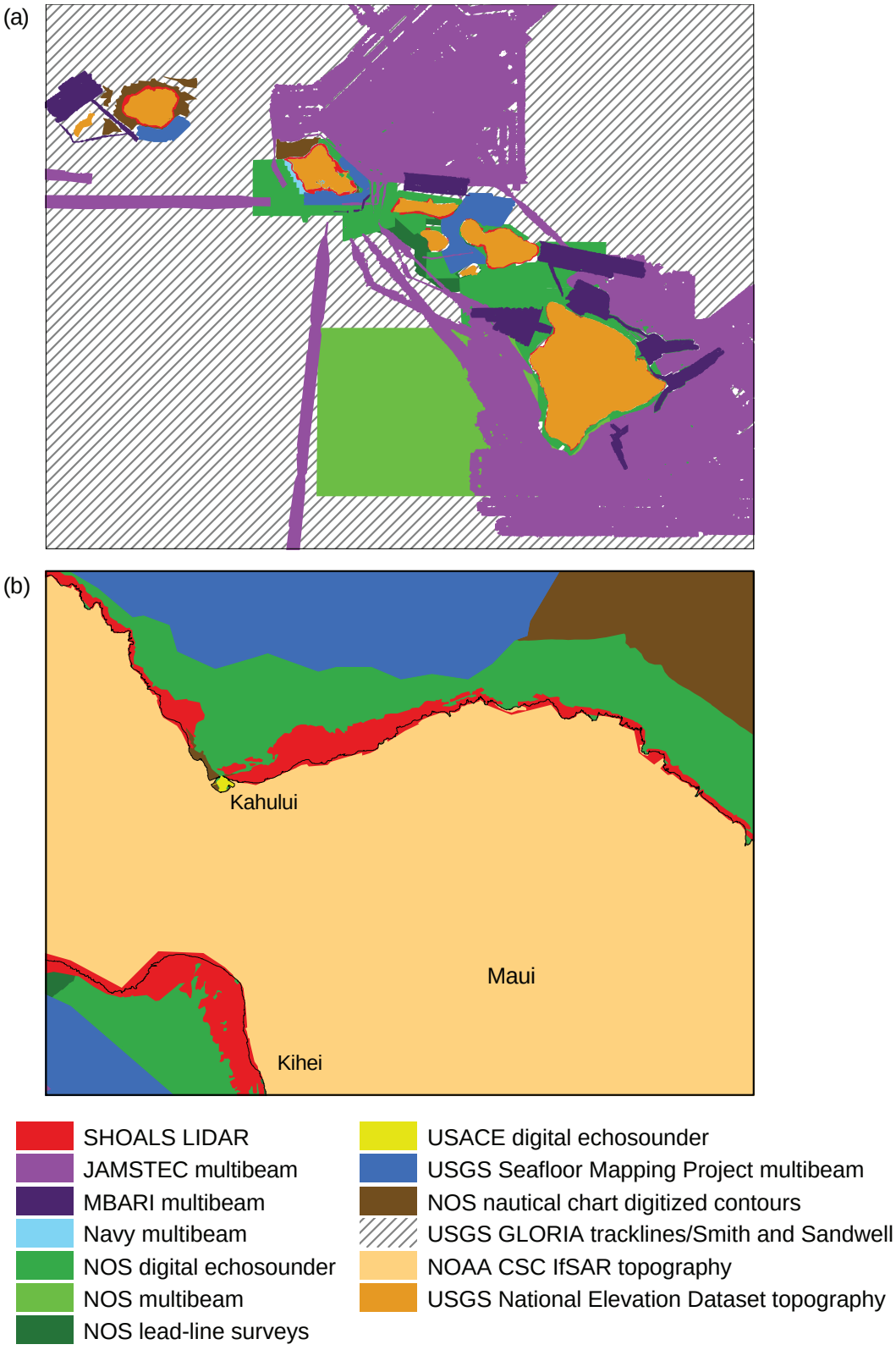

Figure 10: Bathymetric and topographic data source overview. (a) Hawaiian Islands with 6-arc-sec resolution; (b) Maui with 1/3-arc-sec resolution.

Table 2: Data sources used for grid development.

Data Provider	Data Type	Survey Dates	Description
Joint Airborne Lidar Bathymetry Technical Center of Excellence (JALBTCX)	Points	1999–2000	Nearshore bathymetry and topography from SHOALS airborne LIDAR. 1–5-m horizontal resolution.
Monterey Bay Aquarium Research Institute (MBARI)	Grid	1998	Multibeam bathymetric surveys. 10–30-m horizontal resolution.
USGS Pacific Seafloor Mapping Project	Grid	1998	Multibeam bathymetric surveys. 8-m resolution
Japan Agency for Marine-Earth Science and Technology (JAMSTEC)	Grid	1998–2002	Multibeam bathymetric surveys. 150-m horizontal resolution. Multibeam tracklines at varying resolutions.
United States Navy	Point	2000	Multibeam surveys, south and west sides of Oahu
United States Army Corps of Engineers, Honolulu District (USACE)	Point	2000–2005	Digital echosounder surveys in USACE harbor project areas
National Geophysical Data Center (NGDC)	Point	1968–1992	Bathymetric survey data. Multiple technologies, including lead line, digital echosounder, and multibeam.
National Ocean Service (NOS)	Point	1979–1989, 2005	Older bathymetric data points digitized from NOS nautical charts. Recent points imported from Electronic Navigational Charts (ENCs).
Smith and Sandwell (1997)	Point	1997	2-min resolution bathymetry derived from satellite altimetry and ship tracklines.
USGS Geological Long-Range Inclined Asdic (GLORIA)	Point	1986–1988	Sidescan sonar bathymetric surveys in deep-water regions of Hawaii's EEZ.
NOAA Coastal Services Center	Grid	2005	IfSAR (radar altimetry) topographic survey. Gridded to 5-m horizontal resolution.
USGS National Elevation Dataset	Grid	Varies	10-m resolution topographic data derived from USGS DEMs

19381, and 19324. Sounding data from electronic chart (ENC) 19357 was used. This data was included in relatively shallow regions where other data sources were sparse or unavailable, or for quality control of other sources.

- Smith, W.H.F., and D.T. Sandwell, Global seafloor topography from satellite altimetry and ship depth soundings, *Science, 277*, 1957–1962, 26 September 1997. Online reference: `http://topex.ucsd.edu/WWW_html/mar_topo.html`.
- USGS Geological Long-Range Inclined Asdic (GLORIA) surveys. Online data reference: `http://walrus.wr.usgs.gov/infobank/` .
- NOAA Coastal Services Center. `http://www.csc.noaa.gov/`. The IfSAR topographic data was collected and processed for CSC by Intermap Technologies Inc. The data is subject to a restrictive license agreement and is not publicly available.
- USGS National Elevation Dataset. Online reference: `http://seamless.usgs.gov/` .

The SHOALS LIDAR project, which provides high-resolution unified topographic and bathymetric data for the nearshore areas of several Hawaiian Islands, including all of Maui, was essential for accurate modeling of reef and intertidal regions where conventional bathymetric survey data is usually coarse or unavailable. Quality data in this region is especially essential because bathymetric inaccuracies have a great impact on tsunami wave dynamics in shallow water. The 2005 NOAA CSC IfSAR survey of Maui provided similarly valuable high-resolution topography for the entire island, enabling greater confidence in predicting inundation extents. The USGS National Elevation Dataset (NED) was used on other islands outside of the primary study area.

High-resolution gridded datasets derived from multibeam surveys are available for many parts of the archipelago, and were used wherever available. In deep water, where high-resolution multibeam data were not available, the grid was developed by interpolation of a combination of USGS GLORIA surveys and the Smith and Sandwell 2-min global seafloor dataset.

All selected input datasets were converted to the mean high water (MHW) vertical datum as necessary. Bathymetric datasets were converted from the survey tidal datum (usually MLLW or MSL) using offset surfaces interpolated from NOS tide gauges at Kahului, Kawaihae (Hawaii), and Kaunakakai (Molokai). The CSC IfSAR topographic data as obtained was vertically referenced to the GRS80 ellipsoid. It was converted to MHW using an offset surface interpolated from seven National Geodetic Survey (NGS) benchmark stations on Maui that had ellipsoid and tidal heights recorded.

Raw data sources were imported to ESRI ArcGIS-compatible file formats. Horizontal positions were reprojected, where necessary, to the WGS84 horizontal geodetic datum using ArcGIS. In the point datasets, single sounding points that differed substantially from neighboring data were removed. Gridded datasets were checked for extreme values by examination of contour lines, and, where available, by comparison between multiple data sources.

To compile the multiple data sources into a single grid, subsets of the source data were created in the priority order described above. A triangulated irregular network (TIN) was created from the detided vector point data (geodas, usace, csc_lidar). Also added to the TIN were points taken from the edges of the gridded data regions to ensure a smooth interpolated transition between areas with different data sources. This TIN was linearly interpolated using ArcGIS 3D Analyst to produce an intermediate 1-arc-sec and 6-arc-sec raster grid. The gridded datasets were then bilinearly resampled to these resolutions and overlaid on top of the intermediate grids.

4.3 Model Setup

By sub-sampling from the DEMs described in section 4.2, two sets of computational grids were derived, the Kahului Reference Inundation Model (RIM) (Fig. 11) and the Stand-by Inundation Model (SIM) (Figs. 2.a.1, 2.b.3, and 2.c.3). Each set consists of three levels of telescoped grids with increasing resolution. The regional grids cover the major Hawaiian Islands and the

Table 3: MOST setup of Kahului RIM and SIM.

		Reference Inundation Model (RIM)			**Stand-by Inundation Model (SIM)**		
Grid	**Region**	**Coverage Lon. [°E] Lat. [°N]**	**Cell Size [″]**	**Time Step [sec]**	**Coverage Lon. [°E] Lat. [°N]**	**Cell Size [″]**	**Time Step [sec]**
A	Hawaii	199–205.98 18–23	36 (699 × 500)	1.6	199–205.9667 18.0317–22.9967	120 (210 × 150)	12
B	Maui Complex	202.5717–204.098 20.4–21.3933	6 (917 × 597)	0.4	202.8967–204.0967 20.4017–21.255	12 (361 × 257)	1.5
C	Kahului	203.4681–203.71 20.8364–20.975	1/3 (2613 × 1498)	0.2	203.4869–203.6319 20.8674–20.9507	2 (262 × 151)	1.5
Minimum offshore depth [m]		20			20		
Water depth for dry land [m]		0.1			0.1		
Manning coefficient, n		0.01, 0.025, 0.032			0.01, 0.025		
CPU time for a 4-hour simulation		∼41 hours			**<10 minutes**		

coastal grids cover Maui, Lanai, Kahoolawe, and East Molokai. Run-up and inundation simulations are calculated in nearshore grids over the study area. In Fig. 11, the solid boxes in red indicate boundaries of the nested RIM grids while the dashed boxes in red represent the corresponding boundaries of the SIM. Grid details at each level and input parameters are summarized in Table 3.

To reduce numerical instability for certain worst-case scenarios, a large Manning coefficient may be required. The friction coefficient does not change the offshore results. Its effect on model inundation will be discussed in section 4.4.4. For a simulation of a 4-hour event, the optimized SIM takes less than 10 min of CPU time on a Linux system using a single 3.6 GHz Xeon processor, while the RIM takes about 41 hours.

4.4 Results and Discussion

4.4.1 Validation and error estimate

Both the reference inundation model and the stand-by inundation model for Kahului were tested with the 14 historical tsunamis summarized in Table 4. Figure 12 shows the comparisons of observed and modeled time series by RIM and SIM at Kahului tide station and the corresponding wavelet-derived amplitude spectra. The description of the time series of wavelet-derived amplitude spectra can be found in Tang *et al.* (2008).

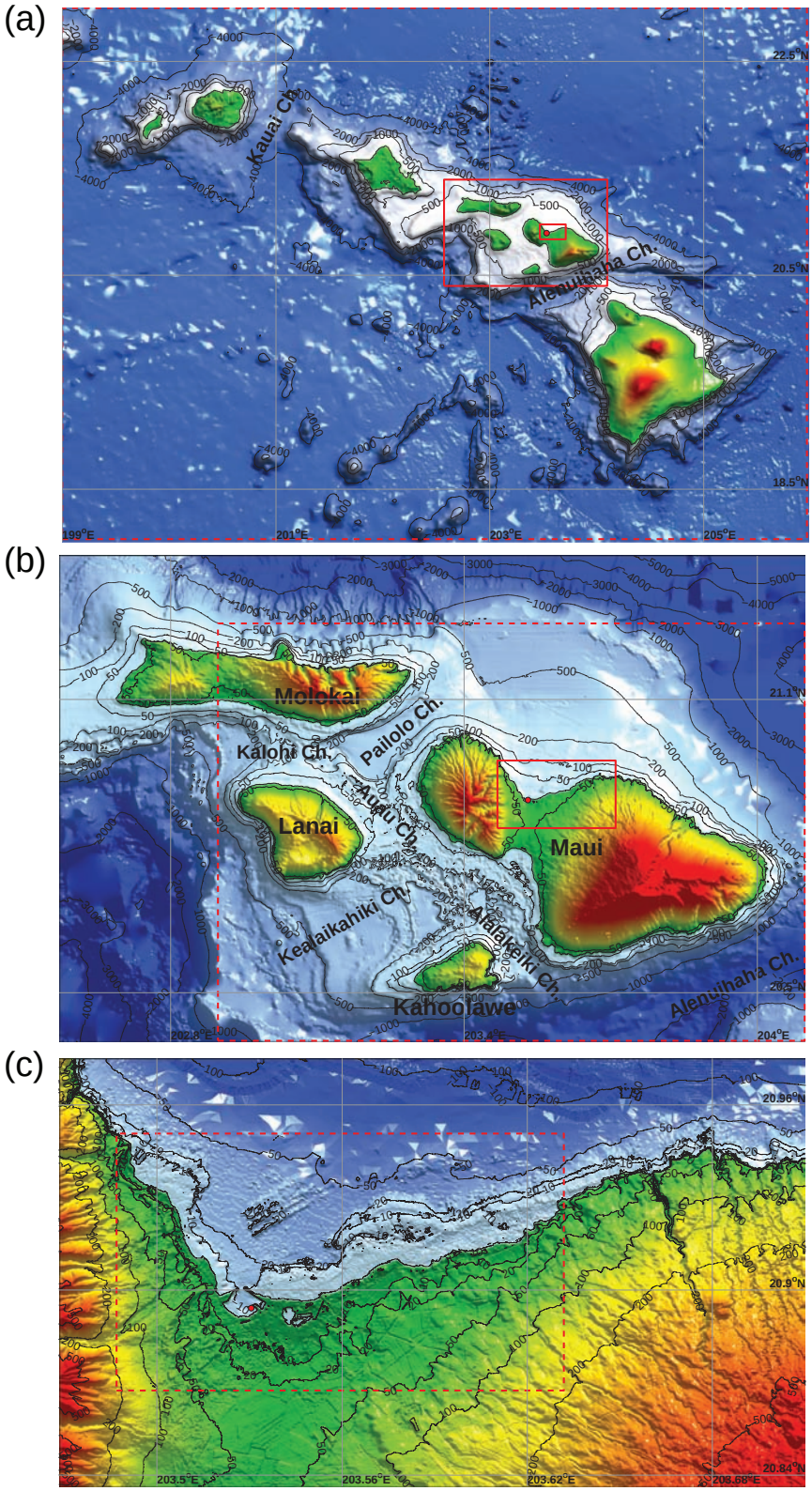

Figure 11: Grid setup of the Kahului Reference Inundation Model (RIM). Solid lines represent the telescoping grids. Dashed lines indicate the corresponding boundaries of the Kahului SIM in Fig 2.

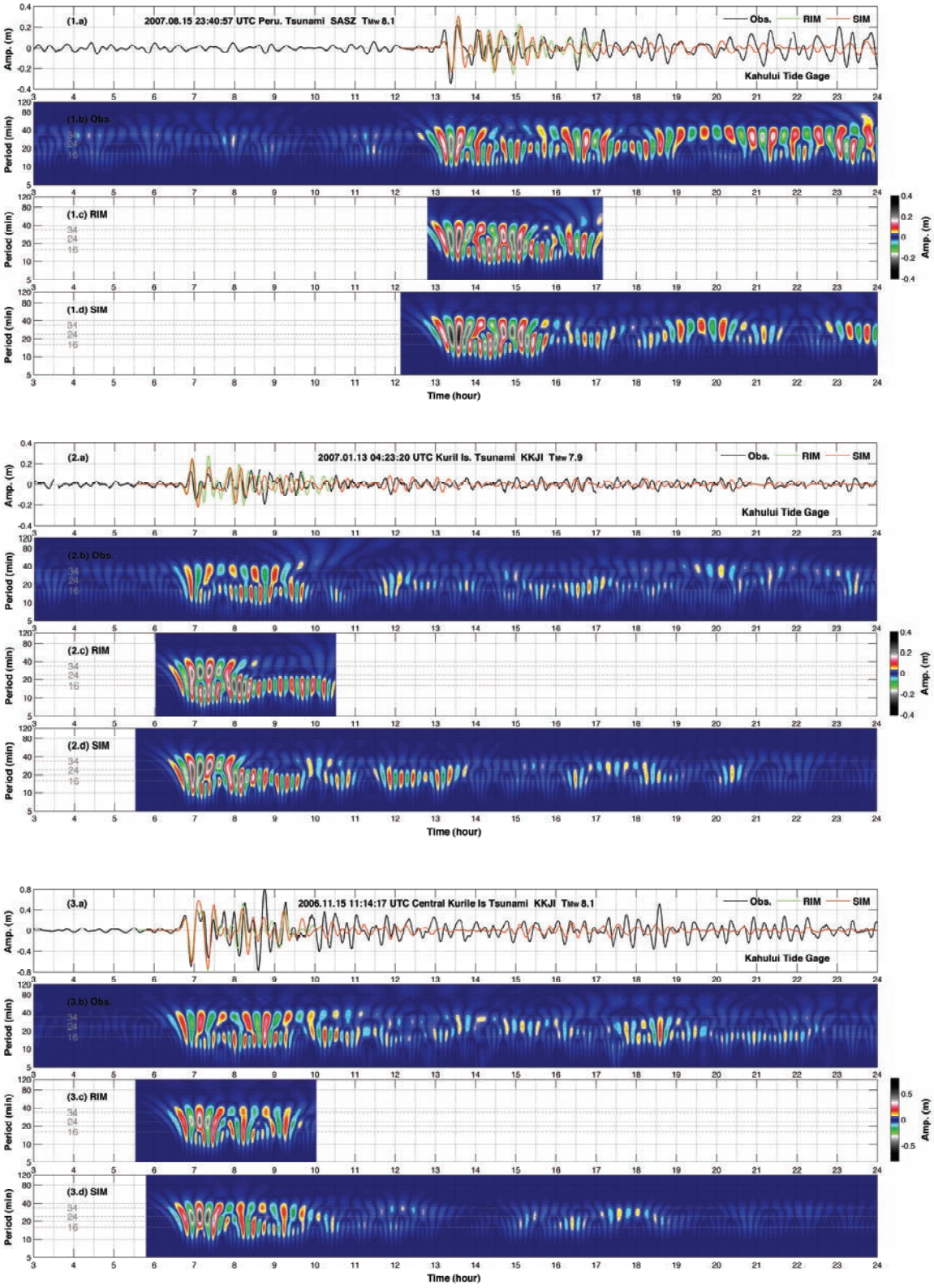

Figure 12, 1–3: Observed and modeled time series of (a) wave amplitudes and (b, c, and d) wavelet-derived amplitude spectra at Kahului tide gage for the 14 historical tsunamis in Table 4. Observations were not available for the 1946, 1952, and 1960 tsunamis.

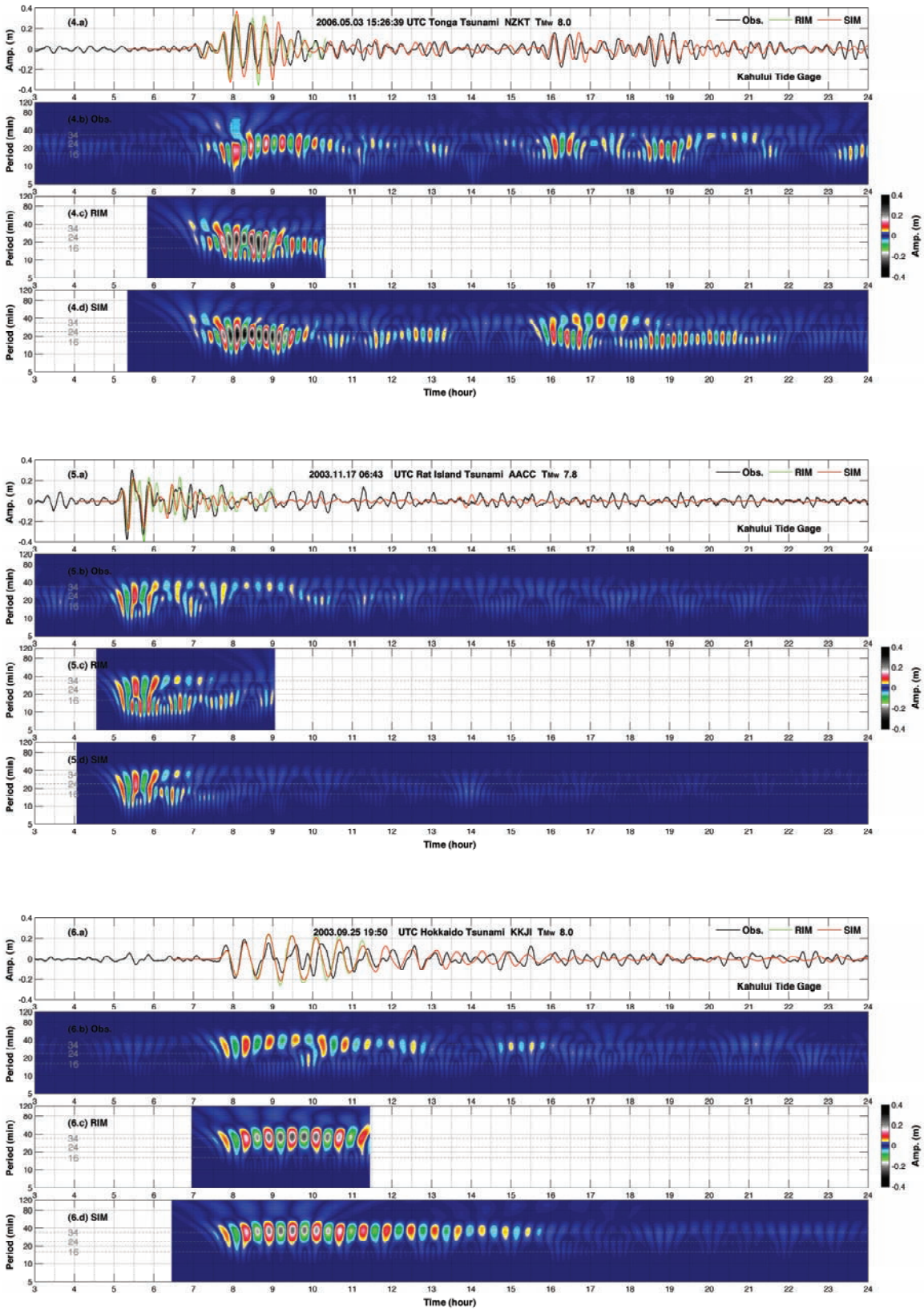

Figure 12, 4–6: Observed and modeled time series of (a) wave amplitudes and (b, c, and d) wavelet-derived amplitude spectra at Kahului tide gage for the 14 historical tsunamis in Table 4. Observations were not available for the 1946, 1952, and 1960 tsunamis.

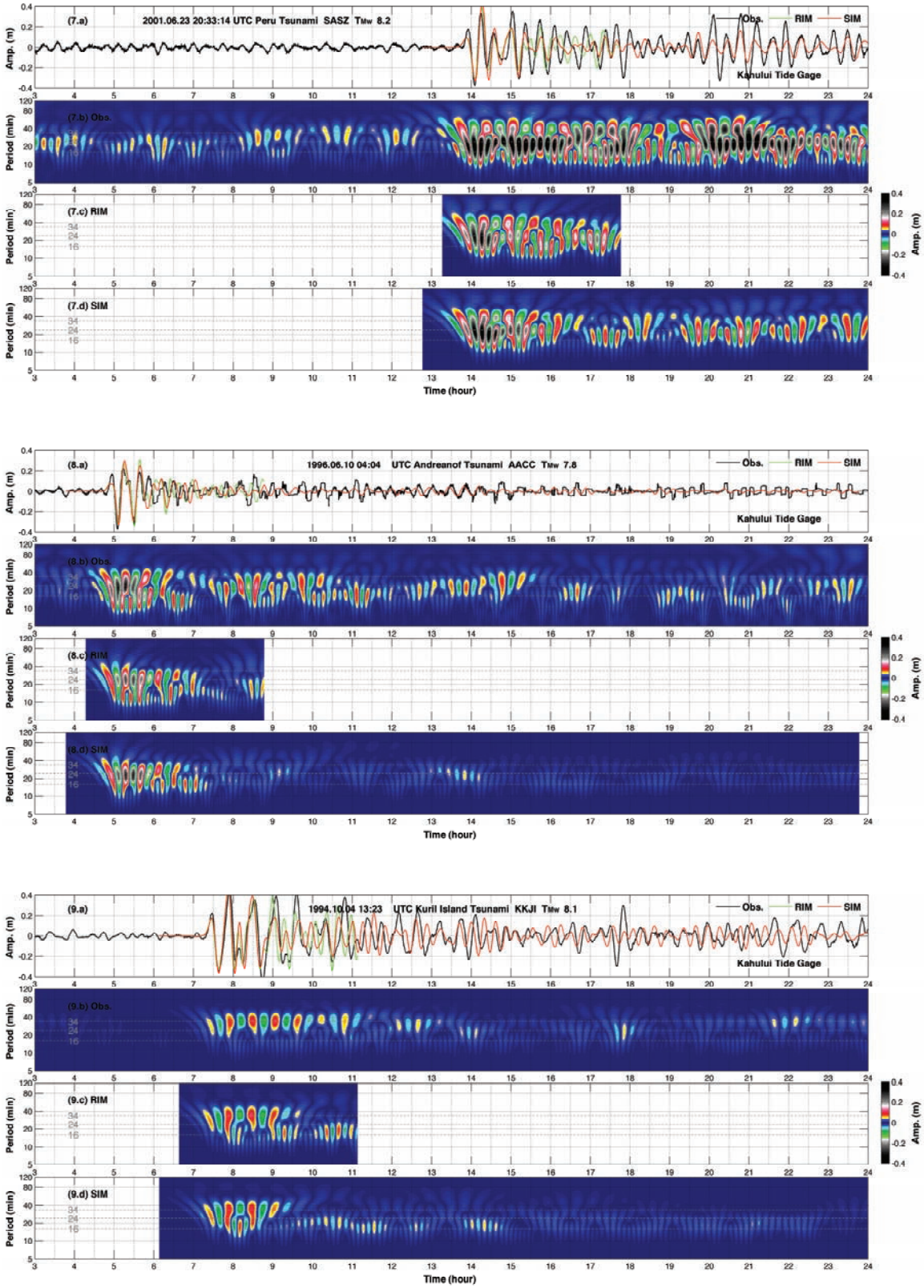

Figure 12, 7–9: Observed and modeled time series of (a) wave amplitudes and (b, c, and d) wavelet-derived amplitude spectra at Kahului tide gage for the 14 historical tsunamis in Table 4. Observations were not available for the 1946, 1952, and 1960 tsunamis.

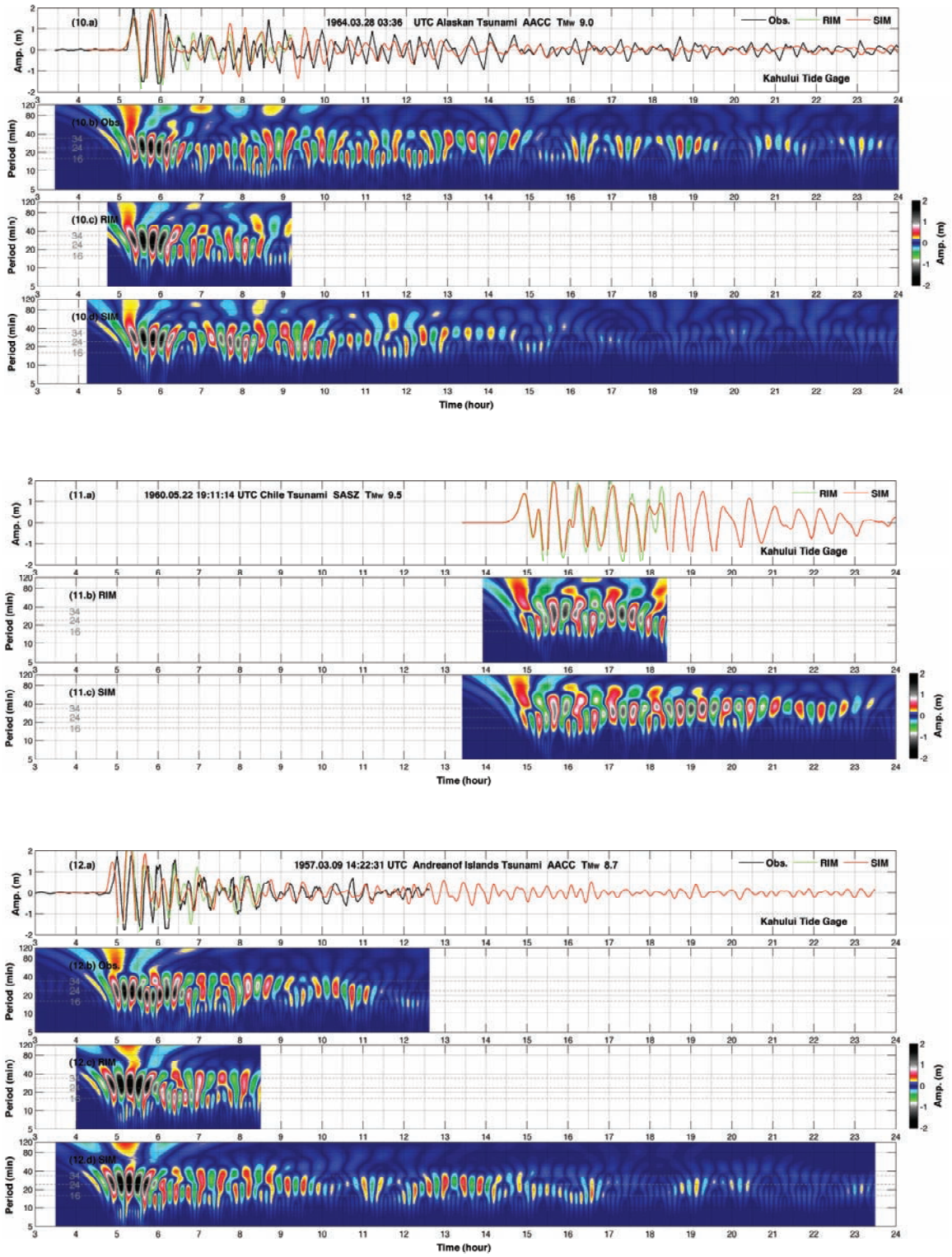

Figure 12, 10–12: Observed and modeled time series of (a) wave amplitudes and (b, c, and d) wavelet-derived amplitude spectra at Kahului tide gage for the 14 historical tsunamis in Table 4. Observations were not available for the 1946, 1952, and 1960 tsunamis.

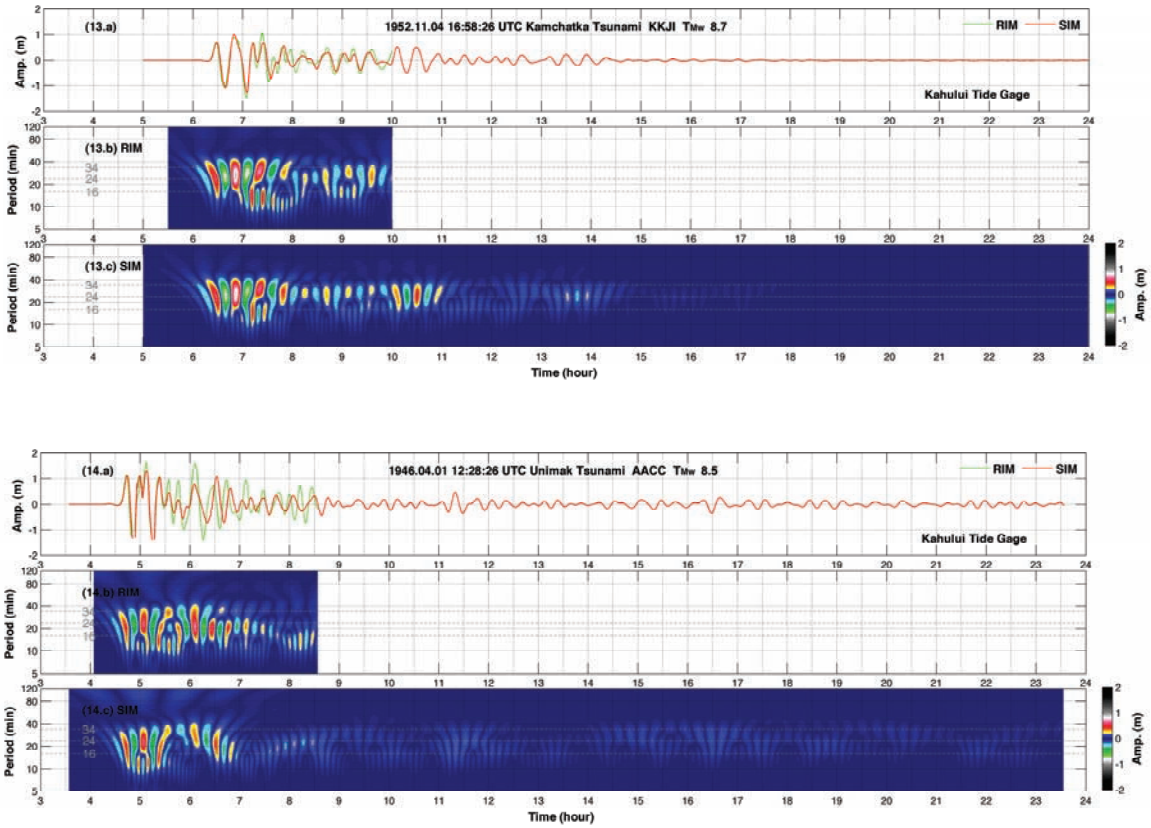

Figure 12, 13–14: Observed and modeled time series of (a) wave amplitudes and (b, c, and d) wavelet-derived amplitude spectra at Kahului tide gage for the 14 historical tsunamis in Table 4. Observations were not available for the 1946, 1952, and 1960 tsunamis.

The most recent event is the 15 August 2007 Peru tsunami. A detailed description of the real-time experimental forecast for this tsunami can be found in Wei *et al.* (2008). At Kahului tide gage, the observed maximum wave height is 56 cm while the forecast is 55 cm. A −12-min adjustment was applied to the modeled time series in Fig. 12.1.a. The modulated amplitude spectrum in Fig. 12.1.b indicates that two groups of oscillations with peak periods near 34 and 16 min exist prior to the arrival of the tsunami.

The 13 January 2007 Kuril Islands earthquake occurred as normal faulting. The tsunami moment magnitude 7.9 was inverted from the first waves recorded at three DARTs, 21414, 46413, and 21413 closest to the epicenter. This tsunami source overestimates the wave heights at Kahului (Fig. 12.2).

The Kuril Islands tsunami of 15 November 2006 provided ample tsunami data and the first test of the NOAA new experimental tsunami forecast system. At Kahului tide station, the largest wave is the 8th wave, which arrived about 2 hours after the first arrival. That is also the latest arrival of the maximum wave among the historical tsunamis studied in this report. The modeled first waves agree well with the observations while the maximum wave height is underestimated (Fig. 12.3.a).

The 3 May 2006 Tonga earthquake generated a tsunami that was detected about 6 hours later by two offshore DARTs located to the south of the Hawaiian Islands, the Dart II (station 51407) and a DART ETD that was under testing. These data were combined with the model propagation database to produce the tsunami source by inversion (Tang *et al.*, 2008). Figure 12.4.a compares the observations at Kahului tide station with model results up to 24 hours after the earthquake. Very good agreement is obtained for the first six waves over 2 hours, including the amplitudes, arrival time, and wave period. The SIM well reproduced the 4th wave as the maximum, which resulted from the combination of far-field and near-field wave scattering and was further amplified by the harbor resonance (Tang *et al.*, 2008). In addition, the Kahului SIM correctly reproduced tsunami waves reflected from the west coast of North America and those scattered by the East Pacific Rise that reached the Hawaiian Islands 16 hours and 18.5 hours, respectively, after the earthquake.

The 17 November Rat Islands tsunami provided the first genuine test of PMEL's forecast methodology (Titov *et al.*, 2005). This tsunami was detected by three DARTs located along the Aleutian Trench. The real-time data was combined with the propagation database to produce the earthquake source by inversion. Titov *et al.* (2005) showed excellent agreement between the model prediction and observed data at Hilo tide gage. The same source was applied here and the results are plotted in Fig. 12.5. Both RIM and SIM correctly produced amplitudes, arrival time, and periods for the first several waves. The wave amplitude decreased quickly and steadily.

The 25 September 2003 Hokkaido earthquake generated tsunami waves of very long periods. Kahului tide station recorded first waves with peak periods near 34 min. The wave amplitude decreased slowly and steadily (Fig. 12.6).

DART buoy 51406, located midway between South America and Hawaii at 8°29′19″S 125°0′20″W, was not deployed until 1 month after the 23 June

Table 4: Tsunami sources and maximum wave height recorded at Kahului tide station for 14 historical tsunamis.

Tsunami No.	Tsunami ID	Tsunami Area	Earthquake Date Time (UTC)	Location Lat (°)	Location Lon (°)	Sub. zone	Seismic moment magnitude (M_w)	Tsunami moment magnitude (T_{Mw})	Obs. H_{max} (m)	Tsunami source
1	200708	Peru	2007.08.15 23:40:57	13.354S	76.509W	SASZ	8.0 (CMT)	8.1	0.57	[1]4.1*a9+4.32*b9
2	200701	Central Kuril Is.	2007.01.13 04:23:20	46.272N	154.455W	KKJI	8.1 (CMT)	7.9	0.33	–3.64*b13
3	200611	Central Kuril Is.	2006.11.15 11:14:17	46.607N	153.230E	KKJI	8.3 (CMT)	8.1	1.47	[1]4*a12+0.5*b12+2*a13+1.5*b13
4	200605	Tonga	2006.05.03 15:26:39	20.13N	174.164W	NZKT	8.0 (CMT)	8.0	0.49	6.6*b29
5	200311	Rat Is.	2003.11.17 06:43:07	51.13N	178.74E	AACC	7.7 (CMT)	7.8	0.66	[1]2.81*b11
6	200309	Hokkaido	2003.09.25 19:50:06	42.4N	143.15E	KKJI	8.3 (CMT)	8.0	0.36	3.6m*(100 × 100 km), 109#rake, 20#dip, 230#strike, 25m depth
7	200106	Peru	2001.06.23 20:33:14	16.14S	73.31W	SASZ	8.4 (CMT)	8.2	0.67	5.70*a15+2.90*b16+1.98*a16
8	199606	Andreanof	1996.06.10 04:04	51.478N	176.847E	AACC	7.9 (CMT)	7.8	0.57	2.40*a15+0.80*b16
9	199410	East Kuril Is.	1994.10.04 13:22:58.3	43.706N	147.328E	KKJI	8.3 (CMT)	8.1	0.69	9.00*a20
10	196403	Alaska	1964.03.28 03:36:14	61.04N	147.73W	AACC	9.2 (USGS)	[2]9.0	[3]>3.46	Tang *et al.* (2006)
11	196005	Chile	1960.05.22 19:11:14	45.88S	76.29W	SASZ	9.5 (Kanamori and Cipar, 1974)		n/a	
12	195703	Andreanof	1957.03.09 14:22:31	51.63N	175.41W	AACC	8.6 (USGS)	[2]8.7	[3]>3.50	31.4*a15+10.6*a16+12.2*a17
13	195211	Kamchatka	1952.11.04 16:58:26.0	52.75N	159.50E	KKJI	9.0 (USGS)	[2]8.7	n/a	
14	194604	Unimak	1946.04.01 12:28	52.75N	163.5E	AACC	8.5 (Lopez and Okal, 2006)	[2]8.5	n/a	7.5*b23+19.7*b24+3.7*b25

1: Forecast tsunami source.
2: Preliminary result.
3: Trough reached gage limit.

2001 Peru tsunami. Therefore, the source for this event was derived based on an inversion of Kahului tide station records using the Kahului SIM. Six tsunami source functions, AB 15 to 17 along the South American subduction zone near the epicenter, were involved. The linear least squares inversion estimates a magnitude of 8.2. In addition to Kahului, it produced good comparisons of first waves at Honolulu and Hilo tide stations. Figure 12.7.a shows that the wave amplitude keeps the same magnitude as the first waves even 14 hours after the first arrival. The underestimation of the model wave heights for the later waves near $t = 20$ hours is also due to the lack of long-period components (Figs. 12.7.a, 12.7.b, and 12.7.c).

Deep-ocean BPR data are also available for two other tsunamis. The inversion of the 10 October 1994 Kuril Islands data was done by using five BPR recordings, while the 10 June 1996 Andreanov used only one. Model results agree quite well with Kahului tide station records for the first several waves (Figs. 12.8 and 12.9), especially the 1994 Kuril Islands tsunami. Though the models missed the second wave, they described the third through sixth large waves along the wave chain well (Fig. 12.9.a).

The limited number of DART buoy records does not include any of the destructive tsunamis described in section 2.1. Previous studies of seismic, geodetic, and water-level data have estimated source parameters for some of the events (Kanamori and Ciper, 1974; Johnson *et al.*, 1994; 1996; Johnson and Satake, 1999). However, those sources are subject to debate and adjustment. Most of the source estimates that have been done are based on low-resolution tsunami propagation models. The SIMs that have been developed at NCTR provide a unique chance to re-investigate the historical sources by inversion of the water level data with the high-resolution quality inundation and propagation models. Preliminary results are available for the 1964, 1957, 1952, and 1946 tsunamis. The fault parameters of the 22 May 1960 Chile tsunami are taken from Kanamori and Ciper (1974). Model results are plotted in Figs. 12.10, 12.11, 12.12, 12.13, and 12.14. The wave amplitude of the 1960 Chile tsunami decayed slowly.

Error estimates of the maximum wave height and arrival of the first wave peak computed by the Kahului SIM for eleven historical tsunamis are presented in Figs. 13.a and 13.b. When the observed maximum wave height is between 0.3 to 0.5 m, the error is within $\pm 50\%$. The low signal-to-noise ratio of the observations and the low ratio of signal to uncertainty from the model setup are the major contributions to the error. When the maximum wave height is greater than 0.5 m, the error reduces to within $\pm 20\%$, which can be attributed mainly to uncertainties from the tsunami source, model setup, and bathymetry. First arrivals in general agree well with the observations, with errors less than $\pm 3\%$ of the travel time. So far, the largest discrepancy between the modeled and observed first arrival time is -12 min for the 200708 Peru tsunami. However, with an earthquake epicenter 460 km to the northwest of the 200708 Peru earthquake, the arrival of the 200106 Peru tsunami has only a -3-min discrepancy. This -12-min arrival discrepancy is currently under investigation.

To further explore the tsunami frequency responses at Kahului, Fig. 13c compares the eleven observed and modeled peak wave periods from the am-

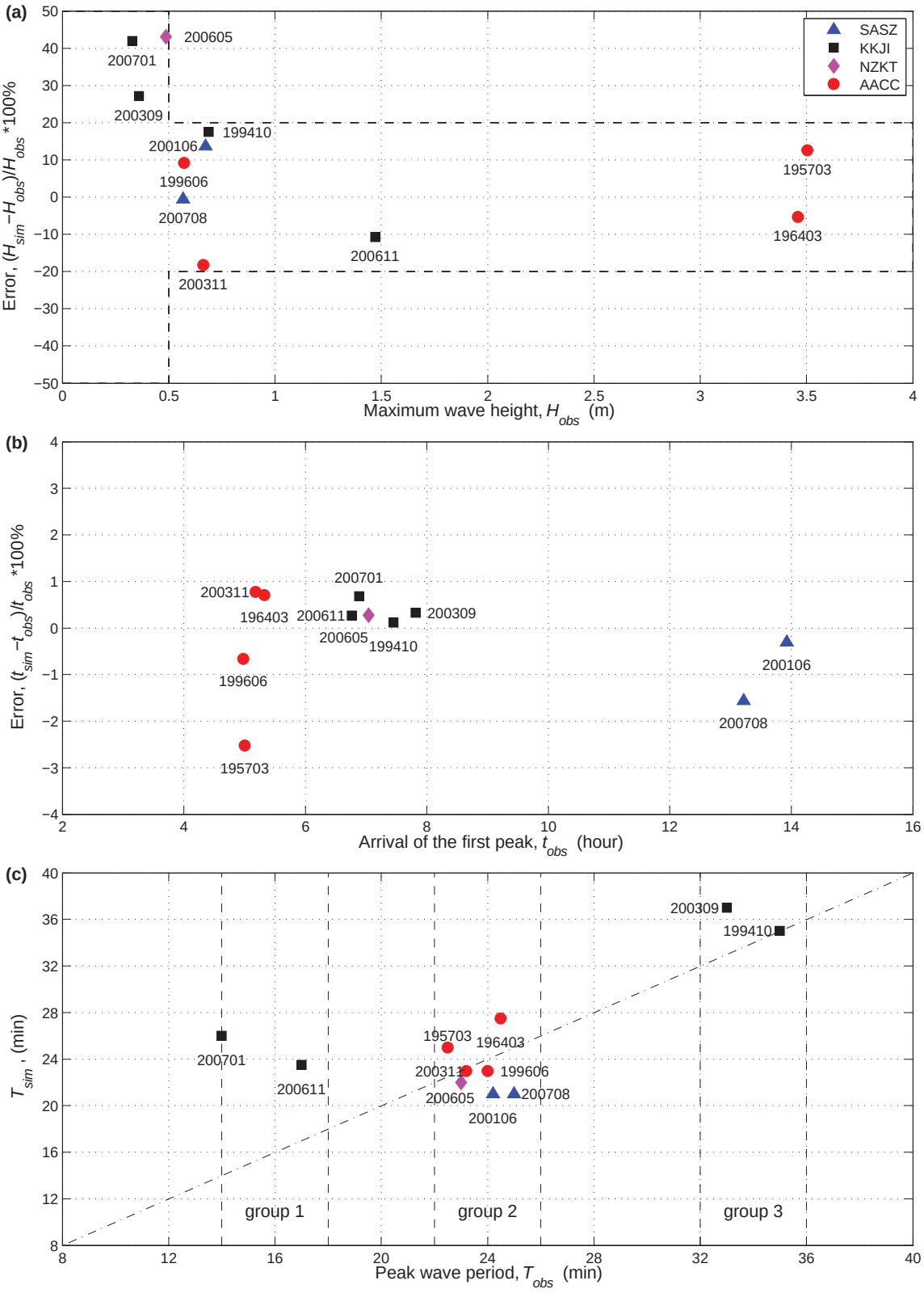

Figure 13: Comparison and error estimation of (a) maximum wave height, (b) arrival of the first wave peak, and (c) peak wave period of observations and model results from the Kahului SIM.

plitude spectra in Fig. 12. The observed peak wave periods fall into one of the three groups of 16-, 24-, or 34-min periods (±2 min). This indicates that the peak wave period is usually one of the local resonant frequencies. An interesting question is, for a particular tsunami, which local frequency will be the peak frequency? Figure 13c indicates that it is mainly related to the geographic location of the earthquakes. Tsunamis originating from the nearby subduction zone earthquakes generate similar peak frequencies at Kahului. For example, the 200611 and 200701 Central Kuril Islands tsunamis have a peak period near 16 min (group 1), while the 199410 West Kuril Islands tsunami and the nearby 2003 Hokkaido tsunami present the same peak period near 34 min (group 3). The remaining seven tsunamis have similar peak wave periods near 24 min (group 2). The Kahului SIM correctly reproduced the peak wave periods within groups 2 and 3. However, there are discrepancies between the modeled and observed peak periods in group 1 for the 200611 and 200701 Kuril Islands tsunamis. Though the 16-min period (group 1) appears in the modeled amplitude spectra, the Kahului SIM for those tsunamis shows a peak period near 24 min (Fig. 12.2 and 12.3). The deep-ocean tsunami observations at DARTs for these two events show that high-frequency components appear in the later wave chains, which were not well resolved in the propagation models. This may cause the peak period computed by the Kahului SIM to be shifted from group 1 to group 2.

To explore the hazard wave conditions over the entire study area, computed maximum water elevation above MHW and maximum velocity of the fourteen tsunamis are plotted in Fig. 14. Both the RIM and SIM produced similar patterns and values. In general, the maximum water elevation exhibits two typical patterns, (1) gradually increasing elevation toward Kahului Harbor, such as the 2003 Hokkaido tsunami (Fig. 14.6); and (2) dramatically increasing elevation near the coastline, such as the 1946 Unimak tsunami (Fig. 4.14). These patterns relate to the tsunami wave periods.

4.4.2 Assessment of potential impact for Kahului from simulated T_{Mw} 7.5, 8.2, 8.7, and 9.3 tsunamis

Located in the middle of the Pacific, Kahului is potentially vulnerable to a variety of Pacific-wide tsunamis. At what magnitude from which location on a subduction zone can a tsunami have a devastating impact on the community? Assessment of the potential impact can provide useful and important information in advance of a real event. The validated Kahului SIM, which was optimized for speed and accuracy, along with the forecast propagation database, provide powerful tools to address this problem.

Even construction of tsunamis of the same magnitude can be enormous with various numbers of tsunami source functions and coefficients. For simplicity, here we apply a uniform coefficient to tsunamis of the same magnitude. Four different magnitudes, T_{Mw} 7.5, 8.2, 8.7, and 9.3 were tested. The details of the simulated tsunami sources and results are summarized in Table 5 and Fig. 15. The maximum water elevation, $\eta_{\max}$, at Kahului tide station from T_{Mw} 7.5 tsunamis computed by the SIM is plotted in bars in Fig. 15b. Color represents the first arrival at the station, which is the

Table 5: Simulated tsunamis for hazard assessment study for Kahului.

	T_{Mw}	Numbers of TSFs	Tsunami source coef.	Lines	Numbers of tests	Range of η_{max} min	Range of η_{max} max	Ratio max/min
1	7.5	1	1	BA	804	0.005 cm	1.90 cm	380
2	7.5	1	1	BA	804	0.05 cm	28.5 cm	570
3	8.2	1	10	B	405	0.01 m	1.55 m	155
4	8.7	6 (3 pairs)	12	BA	381	0.06 m	2.88 m	48
5	9.3	20 (10 pairs)	29	BA	294	0.56 m	9.26 m	17

1: at Kahului offshore from the pre-computed propagation database; 2 to 5: at Kahului station computed by the Kahului SIM.

time of the water level reaching a height of 20% of the first significant peak or trough. Bars in Fig. 15a indicate the maximum elevation at deep water offshore Kahului from the same sources, which are from the propagation database. Figures 15c, d, and e show η_{max} at Kahului tide station from T_{Mw} 8.2, 8.7, and 9.3 tsunamis, respectively. The color represents the difference in time between the arrival of the maximum elevation, t_{max}, and first arrival, t_1.

Tsunami waves in the study area generated by the same magnitude tsunamis from the major subduction zones in the Pacific can vary significantly. Test results in Table 5 show that the ratio of maximum to minimum η_{max} at the station from the same magnitude tsunamis varies from 570 to 17, with T_{Mw} ranging from 7.5 to 9.3. This indicates that moment magnitude alone is inadequate to provide warning guidance for coastal communities, since it contains information related only to the source. This is only the first stage of the three distinct stages of earthquake-generated tsunami, generation, deep-ocean propagation, and coastal transformation. An accurate forecasting and warning system must also take into account the next two stages. SIMs contain local bathymetric and topographic information and utilize the dynamic boundary conditions from the propagation database. They are designed to provide accurate forecasting for site-specific coastal communities and to avoid false alarms resulting from incomplete information. By combining DART inverted tsunami magnitude together with site-specific SIMs, the forecast can completely cover the three distinct stages of the earthquake-generated tsunamis.

Tsunami sources on the Kamchatka and the Aleutian-Alaska-Canada-Cascadia (AACC) subduction zones can generate relatively large waves in Kahului (Fig. 15). One reason could be that Kahului is unprotected from these directions. Late arrival of the maximum wave can be expected from subduction zones in the southwest and west Pacific. Historically, earthquakes at the Kamchatka, Aleutian Alaska, and South America Subduction Zones produced significantly larger tsunami waves. The 1952 Kamchatka, 1946 Unimak, and 1960 Chile earthquakes occurred in these subduction zones, and each had devastating impacts in Kahului. As described by Titov *et al.* (1999), the amplitude of the offshore propagating tsunami could vary significantly by its source location, cylindrical spreading, and directionality of the tsunami wave pattern. Cylindrical spreading decreases tsunami offshore

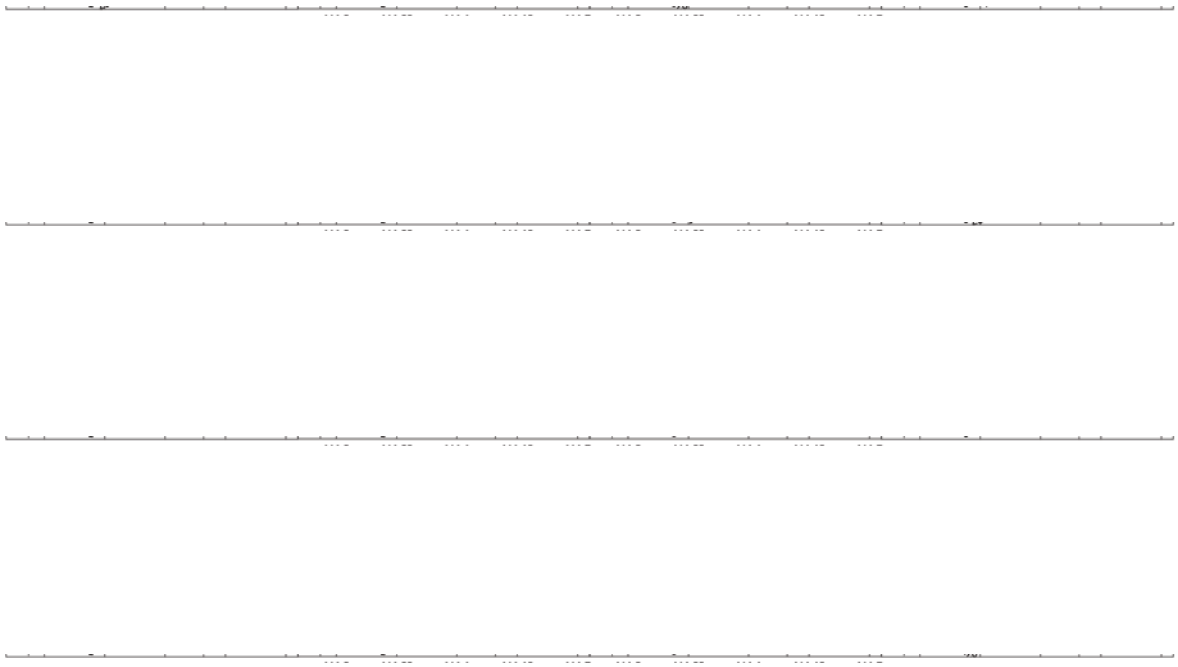

Figure 14, 1–7: Maximum water elevation and maximum velocity computed by the Kahului RIM and SIM for the 14 historical tsunamis.

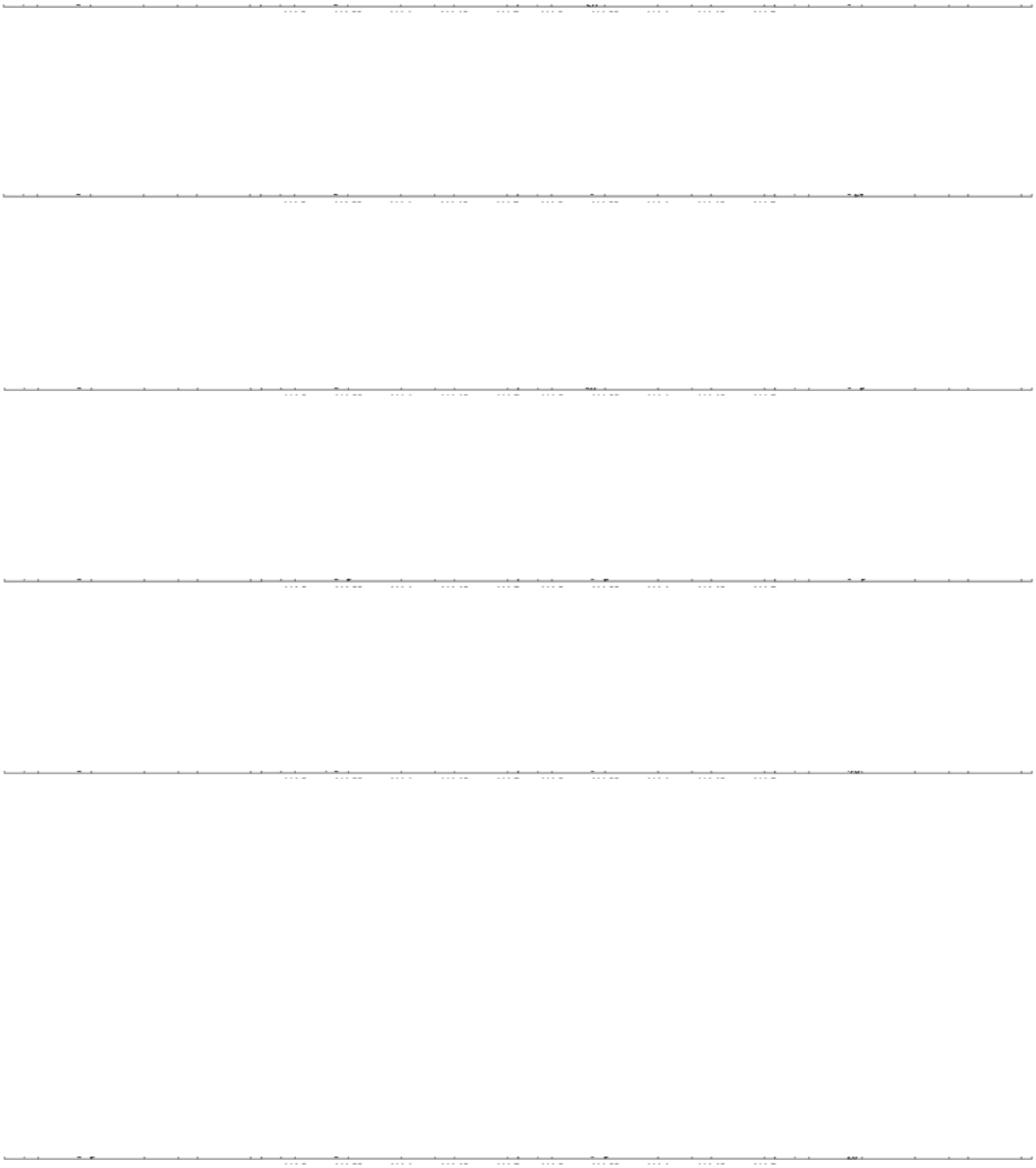

Figure 14, 8–14: Maximum water elevation and maximum velocity computed by the Kahului RIM and SIM for the 14 historical tsunamis.

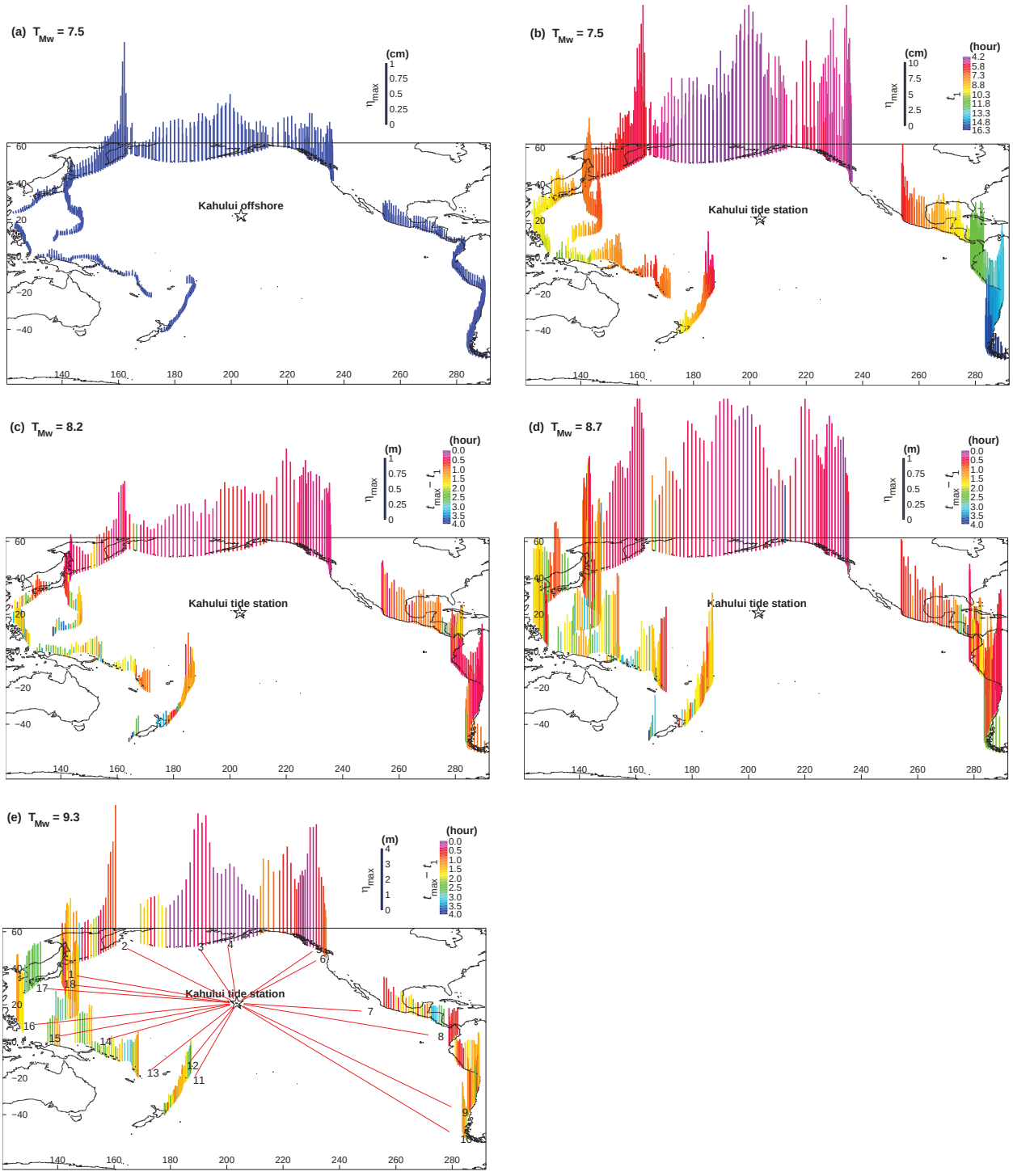

Figure 15: Maximum water elevation at (a) Kahului offshore from the propagation database and (b, c, d, and e) at Kahului tide station computed by the Kahului SIM for simulated T_{Mw} 7.5, 8.2, 8.7, and 9.3 tsunamis. Colors in (b) represent the first arrival at the station. Colors in (c), (d), and (e) represent the difference in time between the arrival of the maximum elevation and the first arrival.

wave amplitude with increasing distance from the source. On the other hand, the shape of a tsunami source and bathymetric profile near the subduction zone makes tsunami energy very directional, with most of the wave energy propagating at a right angle to the earthquake fault. When the path from the tsunami source to Kahului coincides with the propagation direction of the main wave energy and the incident tsunami frequencies are within the right ranges, large tsunami waves can be generated nearshore.

4.4.3 Robustness and stability

Recorded historical tsunamis provide only a limited number of events, from limited locations. More comprehensive test cases of destructive tsunamis with different directionalities are needed to check the stability and robustness of SIMs. A set of 18 simulated T_{Mw} 9.3 tsunamis (Fig. 15e) was selected here for further examination. The SIM results are compared with those from the high-resolution RIM in Figs. 16 and 17. Waveforms computed by the SIM agree well with those from the RIM (Fig. 16). The SIM and RIM compute similar maximum water elevation and inundation in the study area (Fig. 17). These results indicate that the Kahului SIM is capable of providing robust and stable predictions of long duration for Pacific-wide tsunamis.

Tsunami waves in the study area vary significantly for the 18 T_{Mw} 9.3 scenarios. The maximum water elevation at the gage ranges from 1.4 m to 9.3 m for the Tonga (No. 11) and Kamchatka (No. 2) scenarios. These results show the complexity and high nonlinearity of tsunami waves nearshore, which again demonstrate the value of SIMs for providing accurate site-specific forecast details.

4.4.4 Inundation tests

Sensitivity of inundation to the grid resolution for the study area was discussed in section 3.2. In this section, we focus on the sensitivity of inundation computed by the Kahului SIM to the friction coefficient.

Runup data are available for Kahului for the 1946, 1957, 1960, and 1964 tsunamis (Pararas-Carayannis, 1969; Walker, 2004). The 1946 Alaskan tsunami has the most run-up data, with nine points in the study area. Therefore it is selected as the test case. The run-up survey points, after conversion from an assumed original Old Hawaiian Datum to the WGS84 horizontal datum that the topography and shorelines are referenced to, are plotted as black cross symbols in Fig. 18a. The quality of the measurements is ambiguous, since some points fall within the ocean. Figure 18a shows inundation in the Kahului nearshore grid computed from three different Manning coefficients, $n = 0.01$, 0.025, and 0.032. The coefficients generate similar inundation lines for most of the coastline where the slope is relatively steep. However, a small Manning coefficient of 0.01 produces further inundation at several flat areas, such as the southeast area adjacent to Kahului Harbor, including the Maui Mall, the Kanaha Ponds, and the Lower Paia. The waterfront to the southeast of Kahului Harbor has a flat slope of 0.0019 from 2-m topographic contour down to the shoreline. Figure 18b shows the in-

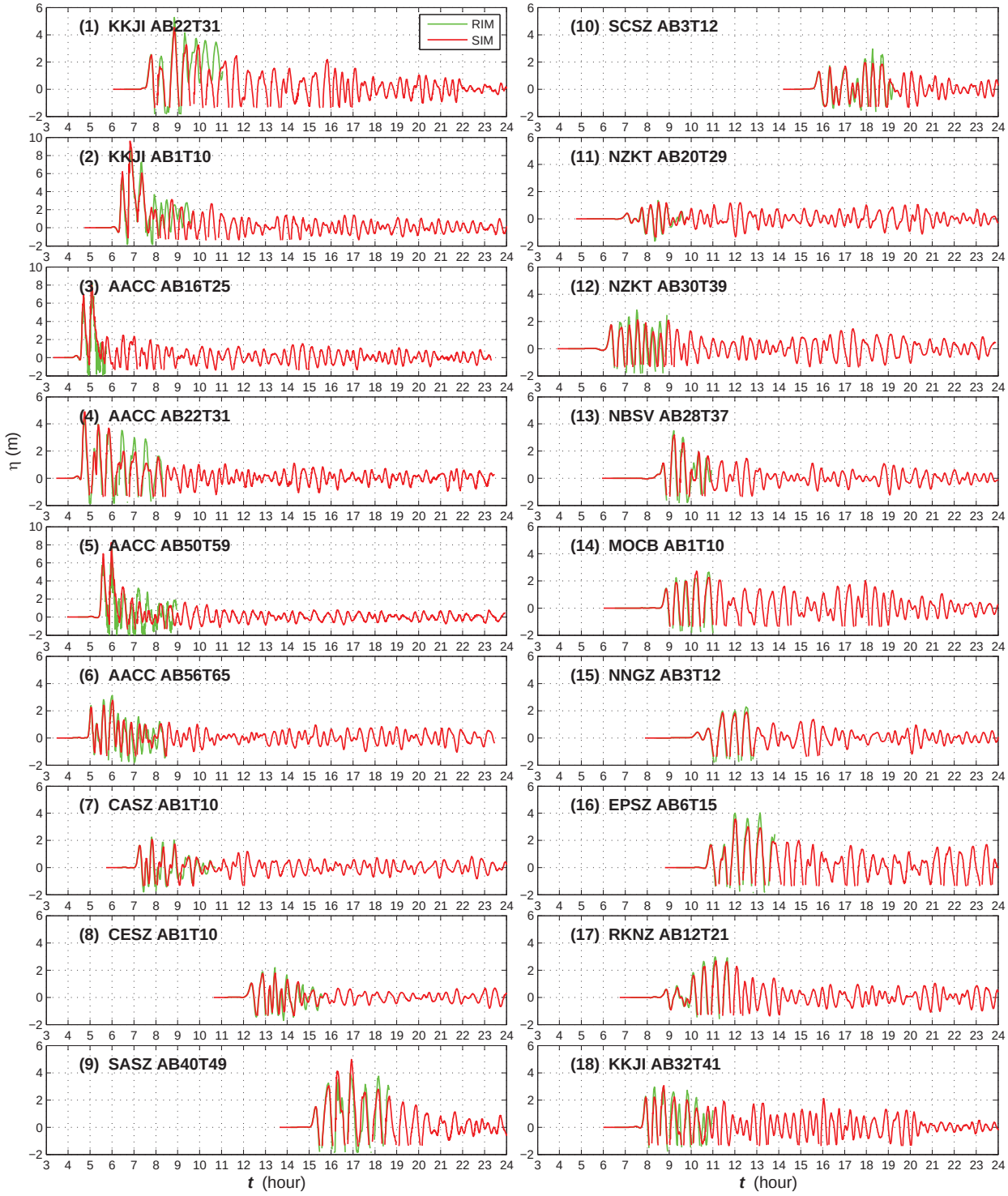

Figure 16: Tsunami time series at the Kahului tide station computed by the RIM and SIM from a set of simulated T_{Mw} 9.3 earthquakes. The label, for example, "KKJI AB22T31" in (1), indicates that the tsunami source is comprised of sources No. 22 to 31 on both A and B lines along the KKJI subduction zone.

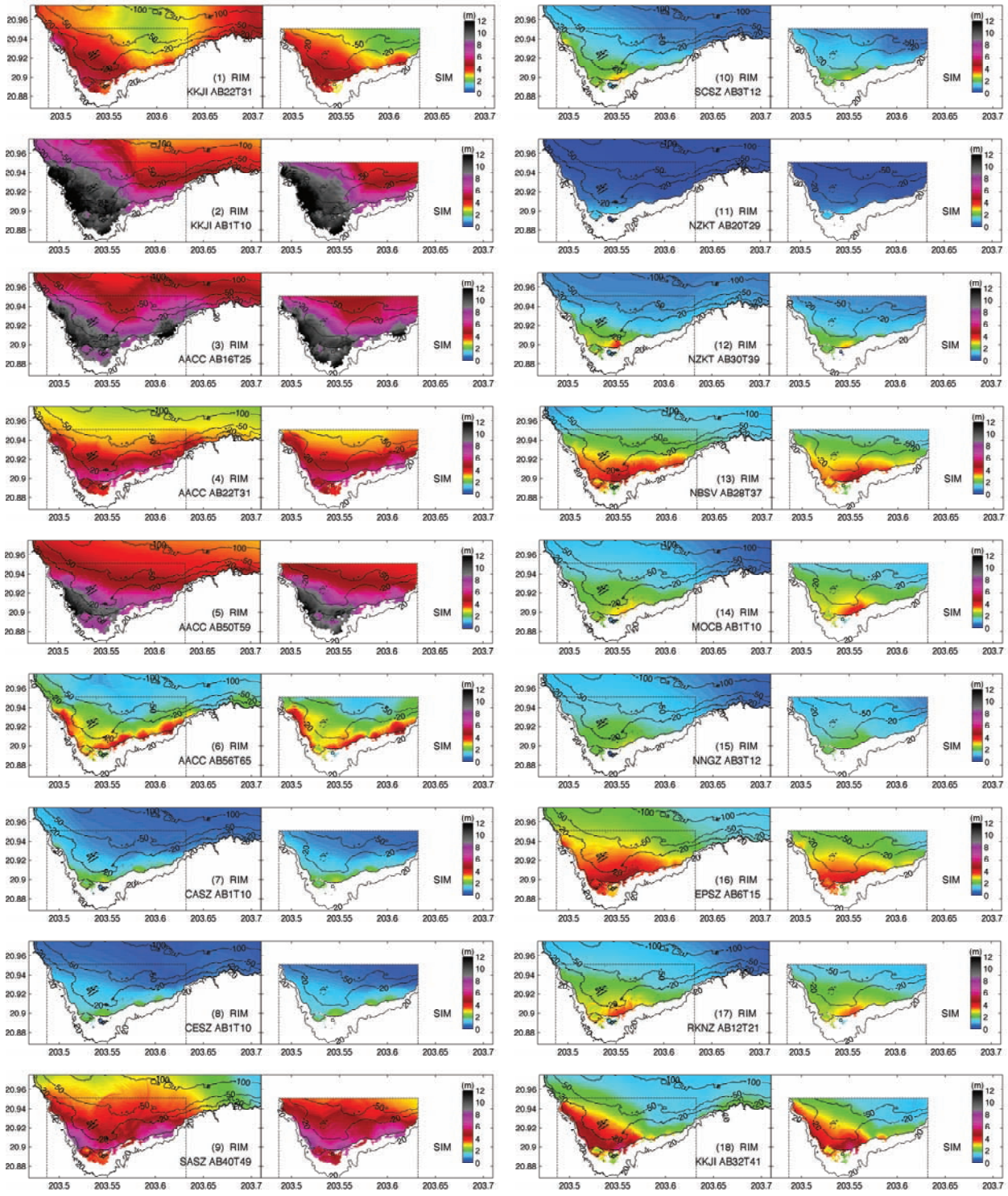

Figure 17: Maximum water elevation in the study area generated by the same set of 18 simulated T_{Mw} 9.3 tsunamis as in Fig. 16.

undation computed with $n = 0.025$ and 0.032 for the T_{Mw} 9.3 Kamchatka scenario (No. 2). Though there are some minor differences at several local areas, the inundation limit agrees well for this test case.

In general, a smaller Manning coefficient can produce further inundation at some flat areas for certain test cases. However, the model can become unstable with a small Manning coefficient for large tsunami waves, such as $n = 0.01$ for the T_{Mw} 9.3 Kamchatka scenario, from which the maximum elevation exceeds 9 m at Kahului tide station. Therefore, for the forecast operational purpose, we suggest $n = 0.01$ to $n = 0.025$. Meanwhile, we suggest considering the waterfront area to the southeast of Kahului Harbor, including the Maui Mall, the Kanaha Ponds, and the Lower Paia, as areas of inundation uncertainty due to lack of measurements to calibrate the Manning coefficient. The computed time series of tsunami elevation at Kahului gage is insensitive to changes in the Manning coefficients.

5. Summary and Conclusions

Sensitivity studies of tsunami wave nearshore characteristics and inundations were conducted for ranges of model grid setups, resolutions, and parameters. Based on these studies, procedures and testing of validation, robustness, and stability were suggested for developing tsunami forecast inundation models (Stand-by Inundation Models, or SIMs).

A SIM was developed for the coastal community of Kahului, Hawaii. The computational grids for the Kahului SIM were derived from the best available bathymetric and topographic data sources. The model was tested with 14 historical tsunamis and different scenarios of simulated T_{Mw} 7.5, 8.2, 8.7, and 9.3 tsunamis based on subduction zone earthquakes in the Pacific. The SIM outputs are compared to both historical water level data and numerical results from a reference inundation model (RIM) of higher resolution.

The accuracy of the maximum wave height computed by the Kahului SIM is greater than 80% when the observed maximum wave height is greater than 0.5 m, and 50% when the observation is between 0.3 to 0.5 m. The error of the modeled first arrivals is within ±3% of the travel time. Wavelet analysis of the observed time series tsunami amplitude at Kahului indicates that the peak wave period mainly falls into one of the three local 16-, 24-, or 34-min resonant periods (±2 min). Which resonance period will be the peak period at Kahului is relevant to the geographic location of the tsunami sources. The optimized SIM can accurately provide a 4-hour site-specified forecast of first wave arrival, amplitudes, and reasonable inundation limit within minutes of receiving tsunami source information constrained by deep-ocean DART measurements. It is also capable of reproducing later tsunami waves reflected or scattered by far-field bathymetry that may arrive hours after the first arrival.

A tsunami could strike Kahului with large waves from the Kamchatka, Alaska-Aleutian, Canada, Cascadia, and South America subduction zones. The Aleutian tsunami has the shortest first arrival at the Kahului gage of

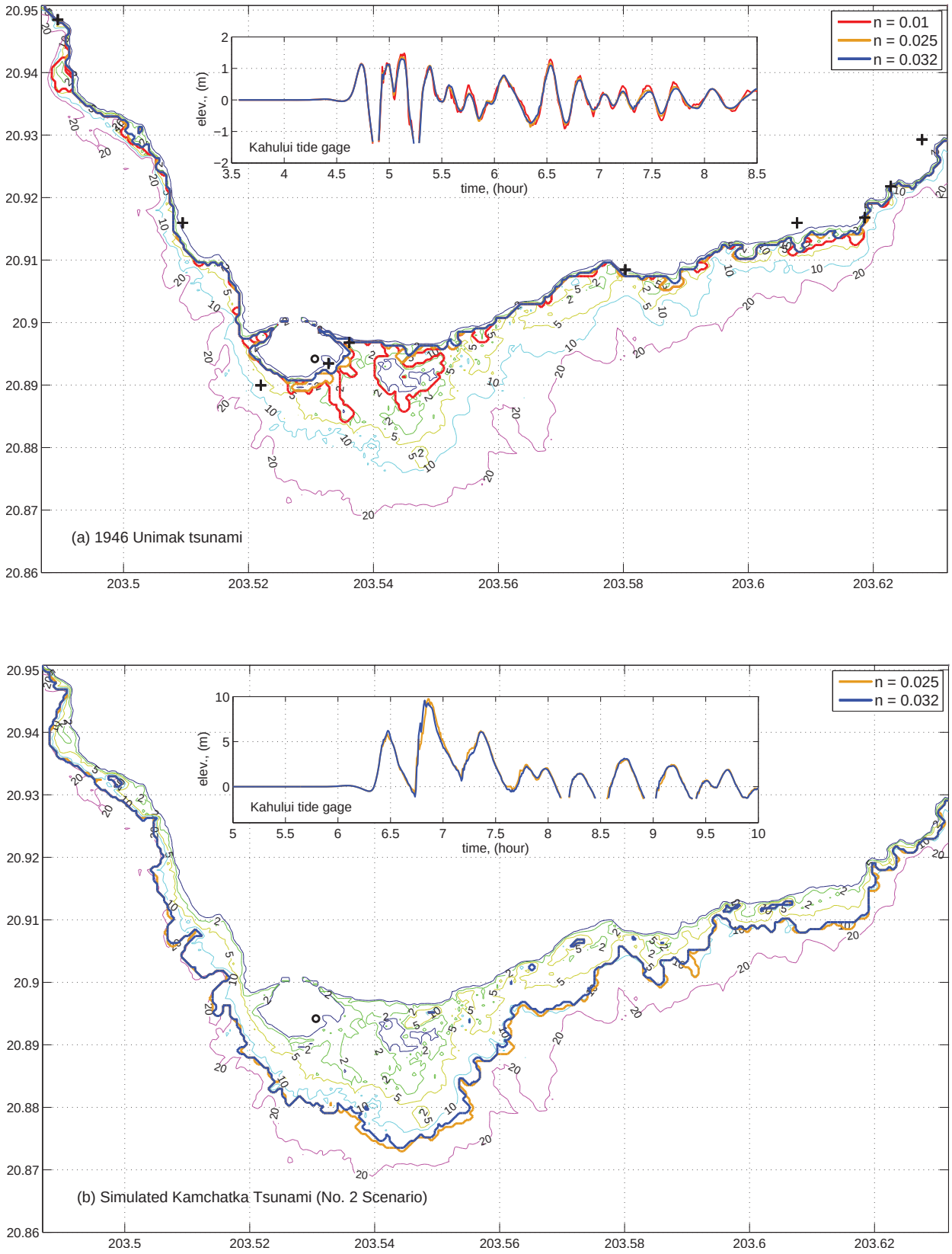

Figure 18: Sensitivity of inundation and time series of tsunami amplitudes computed by the Kahului SIM to Manning coefficients for (a) the 1946 Unimak tsunami, and (b) the simulated T_{Mw} 9.3 Kamchatka tsunami (No. 2).

4.25 hours. Special attention must also be paid to the locations from which the main offshore wave energy propagates toward the Hawaiian Islands, including the East Philippines and Marianas Subduction Zones to the east, and Vanuatu to the southeast. In addition to Kahului Harbor, larger waves may be expected at Waiehu Pt. and Sprecklesville from tsunamis when the peak period is near 16 min or less. The study suggests considering the waterfront area to the southeast of Kahului Harbor, including the Maui Mall, the Kanaha Ponds, and the Lower Paia, as areas of inundation uncertainty due to the lack of measurements to calibrate the friction coefficient for the SIM.

The tsunami hazard assessment study for Kahului shows tsunami waves nearshore can vary significantly from the same magnitude tsunamis from different subduction zones or from different locations on the same subduction zone. As a consequence, the moment magnitude alone is inadequate to provide warning guidance for coastal communities, since it contains information related only to the source. This is only the first stage of the three distinct stages of earthquake-generated tsunami, generation, deep-ocean propagation, and coastal transformation. By including local bathymetry and topography and utilizing the dynamic boundary conditions from the propagation database, SIMs are designed to provide accurate site-specific forecasting for coastal communities, thus avoiding false alarms resulting from incomplete information. Only by combining the DART-constrained tsunami magnitude together with site-specific SIMs can the forecast completely cover the three distinct stages.

6. Acknowledgments

Special thanks to Dr. Elena Tolkova's extensive assistance in pre-processing model input, MOST versioning, and post-processing data. We thank Dr. Mick Spillane for providing information on Kahului offshore; Dr. Harold Mofjeld, Marie Eble, Nazila Merati, Clyde Kakazu, and Allison Allen for assistance with tide gage data; Drs. Robert Weiss, Diego Arcas, and Yong Wei for discussion; Dr. Edison Gica and Jean Newman for assistance with the propagation database. The authors are grateful to Ryan Layne Whitney for his valuable comments, editing, and corrections.

This research is funded by the NOAA Center for Tsunami Research (NCTR), PMEL Contribution #2985. This publication is partially funded by the Joint Institude for the Study of the Atmosphere and Ocean (JISAO) under NOAA Cooperative Agreement No. NA17RJ1232, PMEL Contribution #1310.

7. References

Bernard, E.N., H.O. Mofjeld, V.V. Titov, C.E. Synolakis, and F.I. González (2006): Tsunami: Scientific frontiers, mitigation, forecasting, and policy implications. *Philos. Trans. R. Soc. Lond. A*, *364*(1845), 1898–2007, doi:10.1098/rsta.2006.180.

Bernard, E.N., and V.V. Titov (2007): Improving tsunami forecast skill using deep ocean observations. *Mar. Technol. Soc. J.*, *40*(3), 23–26.

Gica, E., M.C. Spillane, V.V. Titov, C.D. Chamberlin, and J.C. Newman (2008): Development of the forecast propagation database for NOAA's Short-Term Inundation Forecast for Tsunamis (SIFT). NOAA Tech. Memo. OAR PMEL-139, NOAA/Pacific Marine Environmental Laboratory, Seattle, WA, 89 pp.

González, F.I., E.N. Bernard, C. Meinig, M. Eble, H.O. Mofjeld, and S. Stalin (2005): The NTHMP tsunameter network. *Nat. Hazards*, *35*(1), Special Issue, U.S. National Tsunami Hazard Mitigation Program, 25–39.

Gusiakov, V.K. (1978): Static displacement on the surface of an elastic space. Ill-posed problems of mathematical physics and interpretation of geophysical data. *VC SOAN SSSR*, 23–51, Novosibirsk (in Russian).

Johnson, J.M., and K. Satake (1999): Asperity distribution of the 1952 Great Kamchatka earthquake and its relation to future earthquake potential in Kamchatka. *Pure Appl. Geophys.*, *154*(3–4), 541–553.

Johnson, J.M., K. Satake, S.R. Holdahl, and J. Sauber (1996): The 1964 Prince William earthqake: Joint inversion of tsunami and geodetic data. *J. Geophys. Res.*, *101*(B1), 523–532.

Johnson, J.M., Y. Tanioka, L.J. Ruff, K. Satake, H. Kanamori, and L.R. Sykes (1994): The 1957 Great Aleutian Earthquake. *Pure Appl. Geophys.*, *142*(1), 3–28.

Kanamori, H., and J.J. Ciper (1974): Focal process of the great Chilean earthquake, May 22, 1960. *Phys. Earth Planet. In.*, *9*, 128–136.

Little, M. (2006): Personal e-mail communication to NOAA, National Ocean Service Center for Operational Oceanographic, Products and Services.

NOAA/NOS (1991): Next Generation Water Level Measurement System (NGWLMS) Site Design, Preparation, and Installation Manual. NOAA/NOS, January 1991.

Okada, Y. (1985): Surface deformation due to shear and tensile faults in a half-space. *Bull. Seismol. Soc. Am.*, *75*, 1135–1154.

Pararas-Carayannis, G. (1969): Catalog of Tsunamis in The Hawaii Islands. World Data Center A Tsunami, ESSA—Coast and Geodetic Survey, 94 pp.

Salsman, G.G. (1959): The tsunami of March 9, 1957, as recorded at tide stations. U.S. Coast and Geodetic Survey, 18 pp.

Shepard, F.P., G.A. Macdonald, and D.C. Cox (1950): Tsunami of April 1, 1946. *Bull. Scripps Inst. Oceanogr.*, *5*, 391–528.

Soloviev, S.L., Ch. N. Go, and Kh. S. Kim (1992): Catalog of Tsunamis in The Pacific 1969–1982. Results of Researches on the International Geophysical Projects, Soviet Geophysical Committee, Academy of Sciences of the USSR, Moscow, USSR, 208 pp.

Synolakis, C.E., E.N. Bernard, V.V. Titov, U. Kânoğlu, and F.I. González (2007): Standards, criteria, and procedures for NOAA evaluation of tsunami numerical models. NOAA Tech. Memo. ERL PMEL-135, NOAA/Pacific Marine Environmental Laboratory, Seattle, WA, 55 pp.

Tang, L., C. Chamberlin, E. Tolkova, M. Spillane, V.V. Titov, E.N. Bernard, and H.O. Mofjeld (2006): Assessment of potential tsunami impact for Pearl Habor, Hawaii. NOAA Technical Memorandum OAR PMEL-131, NOAA/Pacific Marine Environmental Laboratory, Seattle, WA, 36 pp.

Tang, L., V.V. Titov, Y. Wei, H.O. Mofjeld, M. Spillane, D. Arcas, E.N. Bernard, C. Chamberlin, E. Gica, and J. Newman (2008): Tsunami forecast analysis for the May 2006 Tonga tsunami. *J. Geophys. Res.*, (in review).

Titov, V.V. (2008): Tsunami forecasting. In *The Sea*, E. Bernard, and A. Robinson (eds.), Vol. 15, Harvard University Press, Cambridge, MA, in press.

Titov, V.V., and F.I. González (1997): Implementation and testing of the Method of Splitting Tsunami (MOST) model. NOAA Technical Memorandum ERL PMEL-112, NOAA/Pacific Marine Environmental Laboratory, Seattle, WA, 11 pp.

Titov, V.V., F.I. González, E.N. Bernard, M.C. Eble, H.O. Mofjeld, J.C. Newman, and A.J. Venturato (2005): Real-time tsunami forecasting: Challenges and solutions. *Nat. Hazards*, *35*(1), Special Issue, U.S. National Tsunami Hazard Mitigation Program, 41–58.

Titov, V.V., H.O. Mofjeld, F.I. González, and J.C. Newman (1999): Offshore forecasting of Alaska-Aleutian subduction zone tsunamis in Hawaii. NOAA Technical Memorandum. ERL PMEL-114, NOAA/Pacific Marine Environmental Laboratory, Seattle, WA, 22 pp.

Titov, V.V., H.O. Mofjeld, F.I. González, and J.C. Newman (2001): Offshore forecasting of Alaskan tsunamis in Hawaii. In *Tsunami Research at the End of a Critical Decade*, G.T. Hebenstreit (ed.), Kluwer Academic Publishers, The Netherlands, 75–90.

Titov, V.V., and C.S. Synolakis (1998): Numerical modeling of tidal wave runup. *J. Waterw. Port Coast. Ocean Eng.*, *124*(4), 157–171.

Walker, D.A. (2004): Regional tsunami evacuations for the state of Hawaii: A feasibility study on historical runup data. *Sci. Tsunami Haz.*, *22*(1), 3–22.

Wei, Y., E. Bernard, L. Tang, R. Weiss, V. Titov, C. Moore, M. Spillane, M. Hopkins, and U. Kânoğlu (2008): Real-time experimental forecast of the Peruvian tsunami of August 2007 for U.S. coastlines. *Geophys. Res. Lett.*, *35,* L04609, doi: 10.1029/2007GL032250.